NASA CR135139
NSR 5-1

THE PLASMATRON:

ADVANCED MODE THERMIONIC ENERGY CONVERSION

BY L. K. HANSEN, G. L. HATCH, AND N. S. RASOR

RASOR ASSOCIATES, INCORPORATED

PREPARED FOR

NATIONAL AERONAUTICS AND SPACE ADMINISTRATION

NASA LEWIS RESEARCH CENTER

CONTRACT NAS3-19861

1. Report No. NASA-CR-51	2. Government Accession No.	3. Recipient's Catalog No.
4. Title and Subtitle The Plasmatron: Advanced Mode Thermionic Energy Conversion		5. Report Date November, 1976 6. Performing Organization Code
7. Author(s) L.K. Hansen, G.L. Hatch, N.S. Rasor		8. Performing Organization Report No. NSR 5-1
9 Performing Organization Name and Address Rasor Associates, Inc. 420 Persian Drive Sunnyvale, CA 94086		10. Work Unit No. 11. Contract or Grant No. NAS3-19861
12 Sponsoring Agency Name and Address National Aeronautics and Space Administration Washington, D.C. 20546		13 Type of Report and Period Covered Contractor Report 14 Sponsoring Agency Code

15 Supplementary Notes

Project Manager, James F. Morris, Thermionic and Heat Pipe Section
NASA Lewis Research Center, Cleveland, Ohio 44135

16 Abstract

The plasmatron is a triode thermionic converter, a modification of the more familiar ignited cesium diode thermionic converter. The third electrode is added so that an auxiliary discharge can be used to produce ions for space charge neutralization more efficiently.

The purpose of the present work is to evaluate the plasmatron as a therminic converter, that is, to identify the controlling phenomena of the device, to define those features important for optimum performance, and to determine its practical potential and limitations. To accomplish this a theory of the plasmatron has been developed. Also, a wide range of measurements have been obtained with two versatile, research devices. To gain insight into plasmatron performance, the experimental results are compared with calculations based on the theoretical model of plasmatron operation.

Results are presented which show that the plasma arc drop of the conventional arc (ignited) mode converter can be suppressed by use of an auxiliary ion source. The improved performance, however, is presently limited to low current densities (< 2 amps/cm^2, at practical spacings) because of voltage losses due to plasma resistance. This resistance loss could be suppressed by an increase in the plasma electron temperature or a decrease in spacing.

Plasmatron performance characteristics for both argon and cesium are reported. The argon plasmatron has superior performance.

Results are also presented for magnetic cutoff effects and for current distributing effects. These are shown to be important factors for the design of practical devices.

17. Key Words (Suggested by Author(s))	18 Distribution Statement
Plasmatron Thermionic Converter Auxiliary Ion Source	Unclassified-unlimited

19. Security Classif. (of this report)	20. Security Classif. (of this page)	21. No of Pages	22. Price*
Unclassified	Unclassified		

* For sale by the National Technical Information Service, Springfield, Virginia 22151

TABLE OF CONTENTS

FORWARD

The work reported in this document was performed by Lorin K. Hansen G.L. Hatch, and Ned S. Rasor. The assistance of Cathy Yuen with the calculations is especially appreciated.

The work was performed for the NASA Office of Aeronautics and Space Technology as part of a cooperative program with the ERDA Nuclear Research and Applications Division to study advanced performance thermionic energy conversion. In particular,the plane parallel converter data reported was provided by the ERDA portion of the program.

The encouragement and guidance of James F. Morris, head of the Thermionics and Heat Pipe section of the NASA Lewis Research Center are greatfully acknowledged.

I. SUMMARY

The plasmatron is a triode thermionic converter, a modification of the more familiar ignited cesium diode thermionic converter. The third electrode is added to the device so that an auxiliary discharge can be used to produce ions for space charge neutralization. In the ignited mode diode, ions are produced by operating a low voltage arc between the main electrodes. The resulting arc drop voltage, however, represents a much greater power loss than is actually required to produce the necessary ions. In the plasmatron, ions for neutralization are produced more efficiently, and therefore, the overall performance of the plasmatron is expected to be better than the ignited diode.

The plasmatron was studied briefly in the early 1960's. The purpose of the present work is to reevaluate the plasmatron as a thermionic converter, that is, to identify the controlling phenomena of the device, to better define those features important for optimum performance, and to determine its practical potential and limitations. To accomplish this a theory of the plasmatron has been developed. Also, a wide range of measurements have been obtained with two versatile, research devices. To gain insight into plasmatron performnace, the experimental results are compared with calculations based on the theoretical model of plasmatron operation.

Results are presented which show that the plasma arc drop of the conventional ignited mode converter can be suppressed by use of an auxiliary ion source. The improved performance, however, is presently limited to low current densities (< 2 amps/cm^2, at practical spacings) because of voltage losses due to plasma resistance. This resistance loss could be suppressed by an increase in the plasma electron temperature or a decrease in spacing. These possibilities are presently being studied.

Plasmatron performance characteristics for both argon and cesium are reported. The argon plasmatron has superior performance. The cesium plasma has been found to have an undesirable property (i.e., a small ionization/elastic-scattering cross section ratio) which causes an unacceptable limitation of output current. The extent to which a partial pressure of cesium can be permitted in the device, to produce the appropriate electrode work functions without degrading the performance, has been explored but is not yet clearly determined.

Results are also presented for magnetic cutoff effects and for current distributing effects. These are shown to be important factors for the design of practical devices.

II. INTRODUCTION

One of the primary aims of the current US program in thermionic energy conversion is the improvement of converter performance through the reduction of plasma voltage losses. This reduction in voltage loss results directly in greater converter output voltage. The corresponding increase in converter performance could greatly expand the usefulness of thermionic energy conversion both for space and terrestrial applications. For some applications, the difference between thermionic energy conversion being of minor importance or of major importance is a matter of only a few tenths of a volt output.

Several modificiations of the conventional (cesium diode) thermionic converter have been proposed as a means of achieving advanced performance. These include the hybrid converter, the surface ionization triode, pulsed devices, the ignited triode, etc. [1,2] The plasmatron, the subject of this report, is one form of the ignited triode. An essential feature of the plasmatron is an auxiliary discharge maintained in the space between the main electrodes by an auxiliary electron emitting electrode and an external power supply. This discharge supplies ions for space charge neutralization and therefore is the means for allowing current to pass from the main converter emitter to the collector. In the ignited cesium diode thermionic converter these ions are generated by a low voltage arc between the main electrodes sustained by a small voltage drop ($V_d \simeq 0.5$ volts). As small as this voltage drop is, the full converter current passes through it, and therefore, the drop represents a much greater loss than is actually needed to produce the required ions. An auxiliary discharge independent of the main converter current opens the possibility of more efficient ion production, and therefore, of increased power output.

The motive diagram in Fig. 1 illustrates the general operation of the plasmatron. The auxiliary electrode is biased negative with respect to the emitter. Therefore, electrons from the auxiliary electrode accelerate into the interelectrode space, ionize the gas, and generate a plasma which fills the interelectrode space. The interelectrode space then has sufficient conductivity for a large current to pass from the main emitter to the collector. The plasmatron is only a special case of the ignited triode. Another version, the Gabor triode, uses an auxiliary electron-collecting electrode rather than an auxiliary electron-emitting electrode.

The plasmatron as a thermionic converter was studied briefly by several workers in the early 1960's [3-6]. These early investigations outlined the basic features of the plasmatron, but many questions important to possible application of the device were left unanswered. It is the purpose of this report to reevaluate the plasmatron as a thermionic converter and to better define those features important to optimum performance.

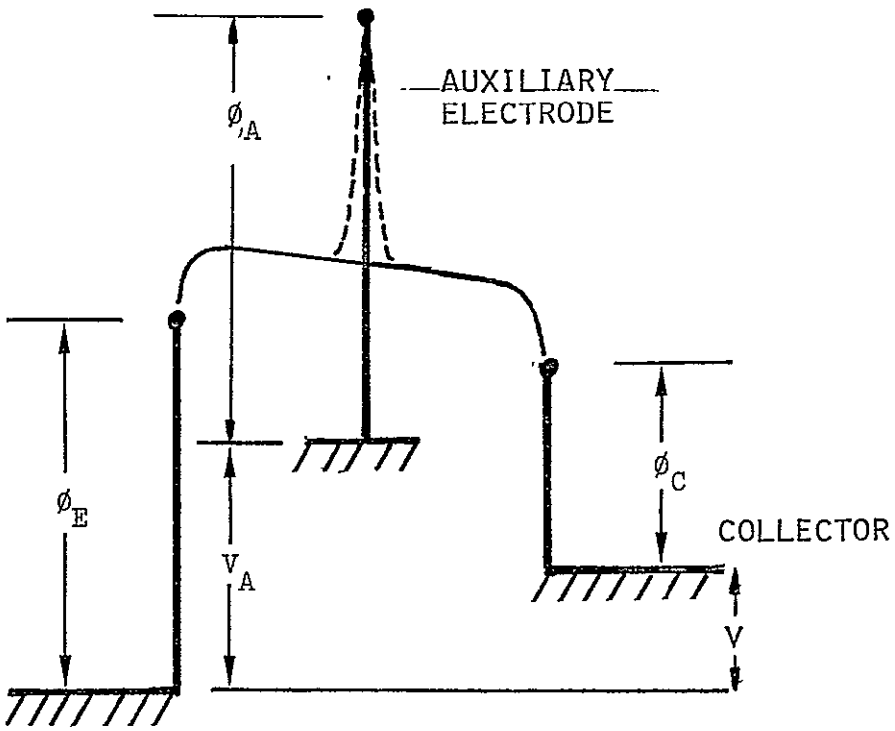

Fig. 1 Motive Diagram and Nomenclatures for the Plasmatron (ϕ_E, ϕ_C, and ϕ_A are the emitter, collector, and auxiliary electrode work functions, V_A and V are the auxiliary electrode bias and output voltages).

III. EXPERIMENTAL APPARATUS

A variety of questions need to be answered in order to evaluate the plasmatron as an energy converter. There are questions about the effects of geometry, pressure, spacing, gas species, enhancement spreading, magnetic fields, etc. These effects need to be understood in order to define the limitations and possibilities of the device. Corresponding to this variety of required measurements there is a need for versatility in the experimental apparatus. To provide this versatility the present study has used a multipurpose converter test stand in which various converter electrode configurations can be introduced as demountable assemblies mounted on standard 4 inch vacuum flanges. This arrangement allows easy access to converter assemblies for quick repair and configuration changes.

Two demountable converters have been built for the present program; one a plane-parallel device, the other a cylindrical device. The essentials of the demountable, plane-parallel converter are shown in Fig. 2, the cylindrical converter in Fig. 3.

As can be seen in Fig. 2, the plane parallel device uses a straight wire through the interelectrode space for the auxiliary electrode. The wire is of tungsten. Its temperature can be raised by passing a current through it. This plasmatron configuration has the advantage of simplicity, but lacks symmetry about the auxiliary electrode. The main emitter is a molybdenum structure with an impregnated-dispenser, planar emitting surface. The emitter is heated by radiation from a heater filament. The spacing from emitter to nickel collector is maintained by alumina spacers. Three probes (auxiliary collectors) mounted flush with the collector surface are used to measure the output current distribution about the auxiliary electrode. The whole assembly of Fig. 2 is mounted on a 4 inch vacuum flange or base plate. A variety of metal-to-ceramic feedthroughs provide electrical and thermocouple connections through the baseplate.

The cylindrical converter is shown in Fig. 3. As the figure shows, this converter also is mounted on a standard vacuum flange. The emitter again is a molybdenum structure with a dispenser emitting surface. However, it is heated by electron bombardment which allows a wider range of temperatures to be obtained. The collector material is stainless steel. The auxiliary electrode is formed from two directly-heated tungsten wires which, together, loop the emitter in

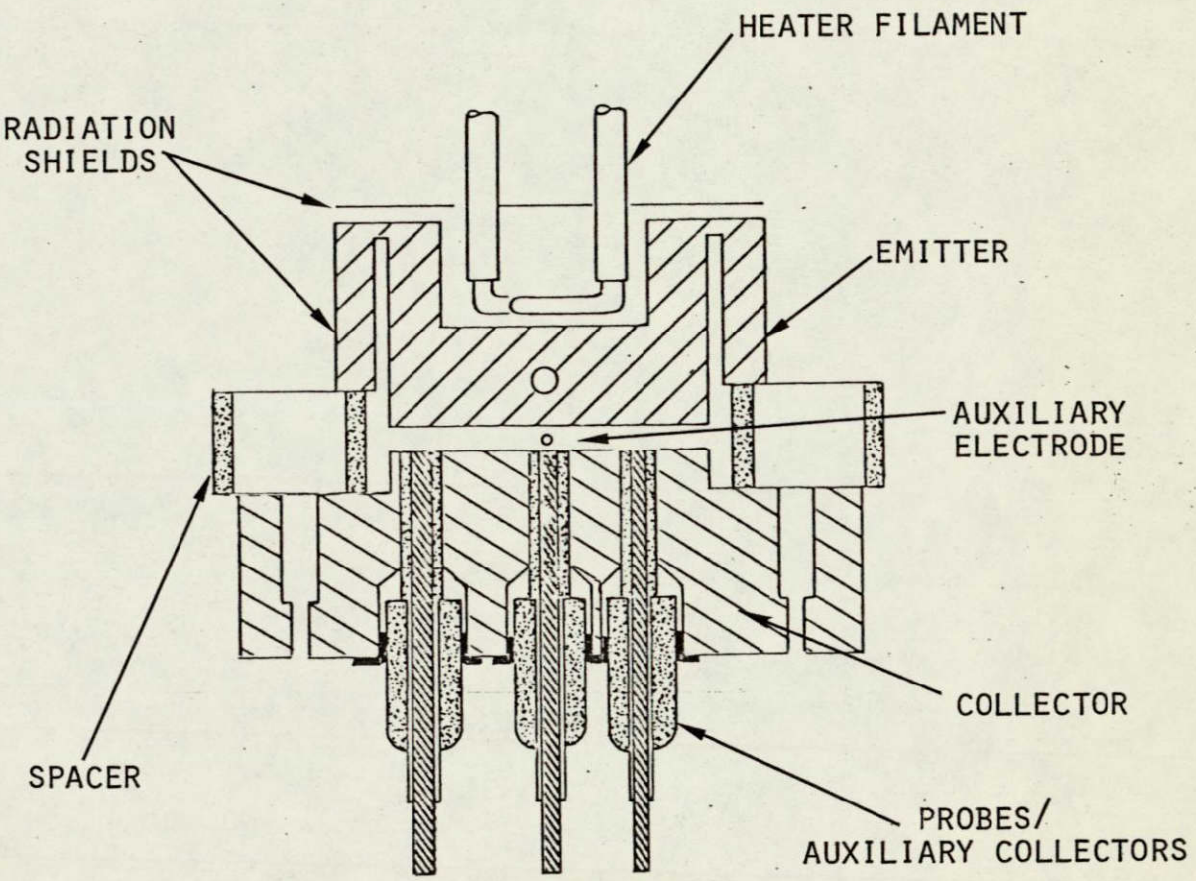

Fig. 2 Demountable Plasmatron Converter With Plane Parallel Electrodes

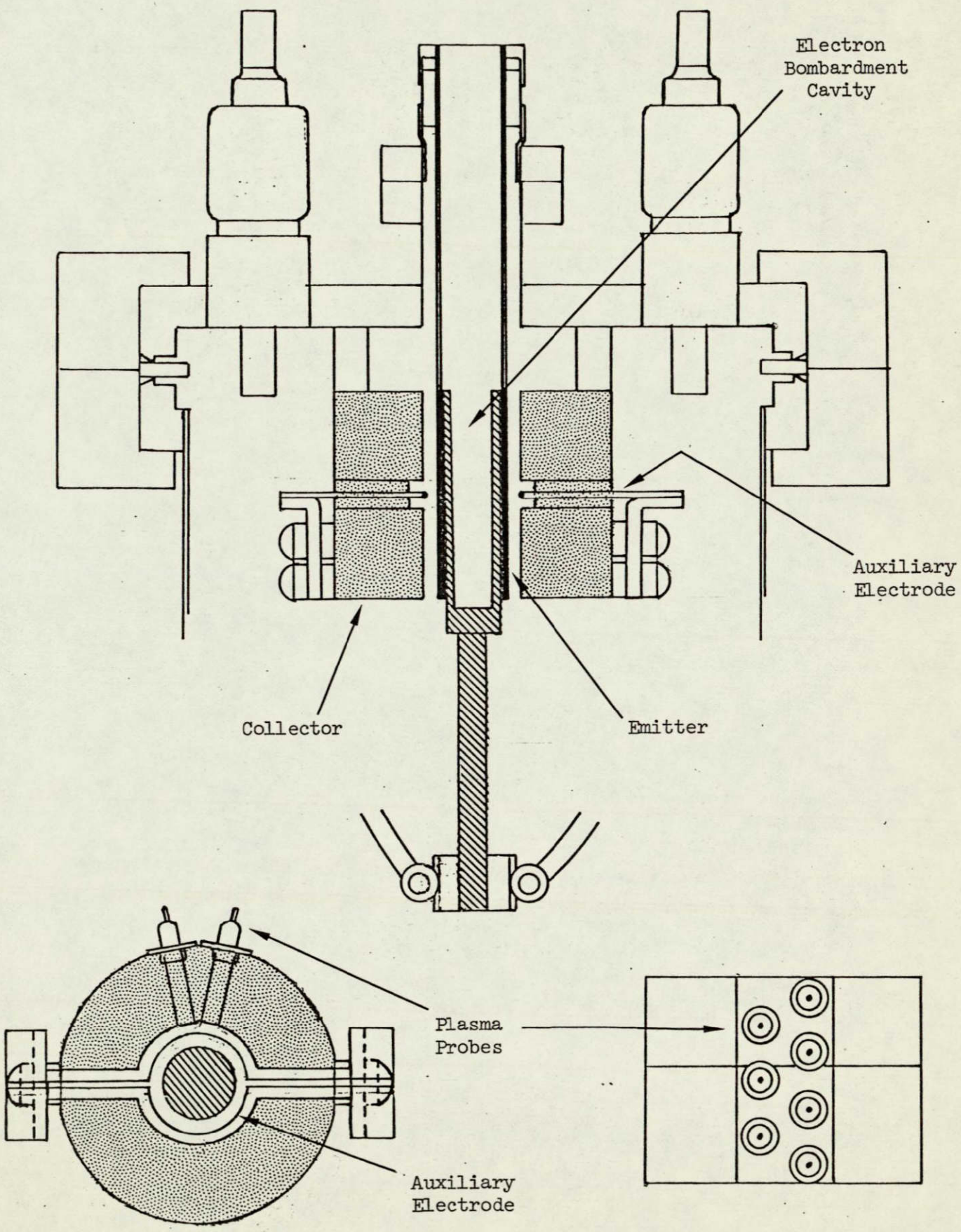

Fig. 3 Demountable Plasmatron Converter With Cylindrical Electrodes

its center plane (a cross sectional is shown in Fig. 3b). The wires have been annealed in the appropriate shape to prevent relaxations which might short the auxiliary electrode to the main electrodes. Seven probes or auxiliary collectors are mounted flush with the collector surface to measure output current distribution. The central probe is directly under the auxiliary electrode. Three additional probes are mounted in each axial direction from the auxiliary electrode (see Fig. 3c). Because of the symmetry of this device, edge effects are minimized in the enhanced-current region. The use of long leads on the auxiliary electrode helps to achieve a uniform temperature for that part of the electrode circling the emitter. For most of the data presented here, ambient temperature (i.e., zero auxiliary electrode heating current) was sufficient to give the emission needed.

A unique feature of this device is the double-ended emitter lead. Current can be passed lengthwise along the emitter, generating an azimuthal magnetic field in the interelectrode space. This allows evaluation of the effect of magnetic field on the magnitude and the distribution of the output current. These effects can be significant in large-current, practical devices.

The use of dispenser emitters in both experimental converters has the advantage that their work function is independent of cesium pressure. Therefore, the plasma properties of the plasmatron can be studied independent of electrode phenomena. Whatever is found concerning these plasma properties, the electrodes needed for a practical device can be identified and chosen accordingly.

The converter test chamber is shown in Fig. 4. The complete converter test stand is shown in Fig. 5. The converter is mounted on the top vacuum flange. The chamber has a sapphire window for observation of the discharge. An all-metal valve permits fast bake-out of in-place devices. The cesium reservoir can be continuously pumped for removal of background gases. Cesium as well as other gases can be introduced through a gas-handling system (shown in Fig, 6). Whatever the gas or gas mixture, the pressure can be measured with a capacitance manometer in the external gas-handling system. A hot-titanium purifier is used to clean-up noble gases before injecting them into the test chamber.

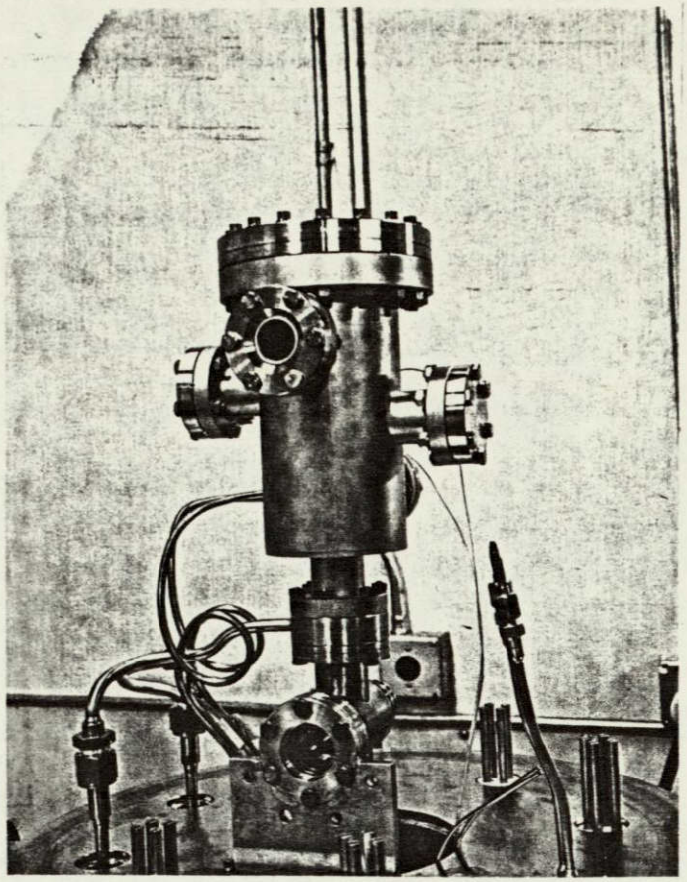

Fig. 4 Experimental Test Chamber

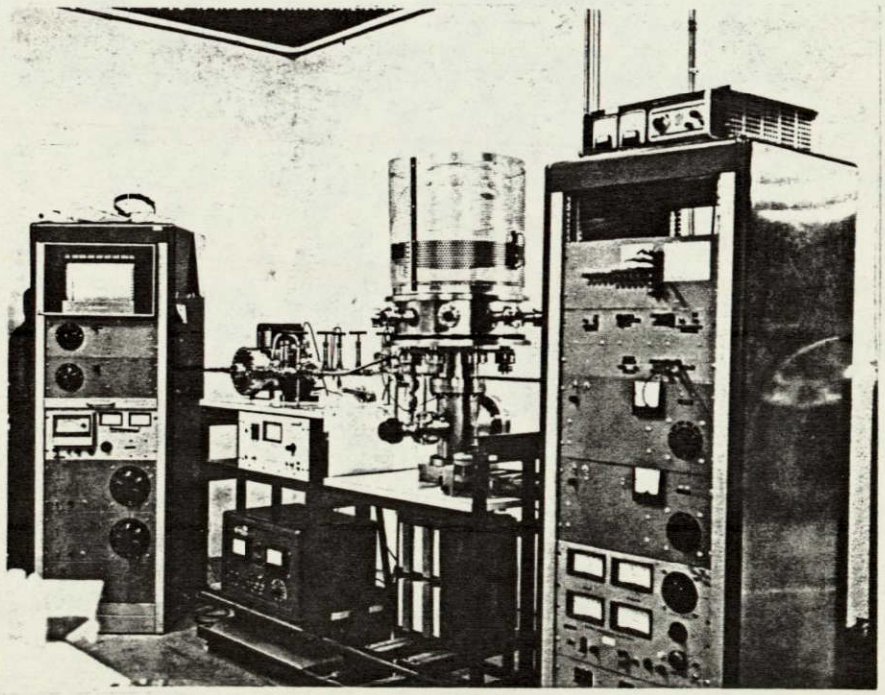

Fig. 5 Demountable Converter Test Stand

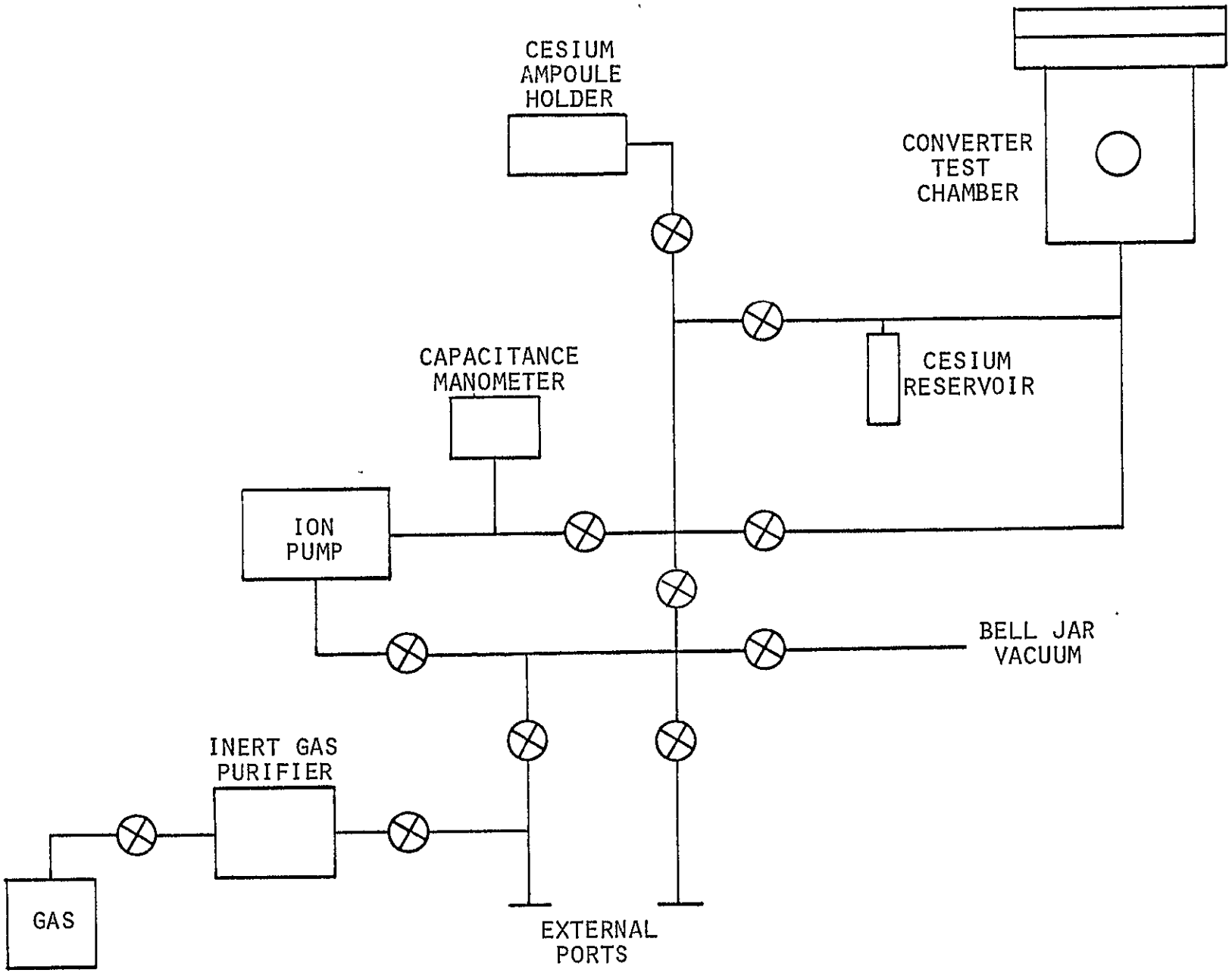

Fig. 6 Gas-Handling System For Demountalbe Converter Test Stand

IV. ANALYSIS OF PLASMATRON PERFORMANCE

Introduction

The evaluation of the plasmatron as a practical device requires not only adequate experimental data, but also a tractable theory of plasmatron operation. With such a theory, calculated performance characteristics can be compared with the experimental data. From these comparisons, the basic dominant phenomena of the plasmatron can be identified and the magnitude of various effects estimated. Also, if there is good agreement between calculated and experimental characteristics, it becomes a simple matter, with a calculator or computer, to broadly survey the effect of various operating conditions on plasmatron performance. Such a theory and such a calculational program is described in the present chapter.

The plasmatron is inherently more complicated than the usual unignited or ignited mode diode converters. There is additional complexity in the geometry because of the third electrode. The interelectrode plasma is also more complex. In addition to the usual low-energy conduction electrons, there is a high-energy beam of ionizing electrons. These two electron groups interact simultaneously with the plasma and with each other. Another complexity arises because the plasmatron is usually operated at low pressure, that is, where the spacing is the same order of magnitude as electron and ion mean free paths. The device is operated in this condition because, at lower pressures, the ionization in the auxiliary discharge becomes inefficient, and at higher pressures, the converter current drops because of electron backscatter to the emitter. Analysis is difficult for this low pressure operation, because there are too many collisions for a simplifying, collisionless approximation to be valid, yet insufficient electron-neutral collisions to justify the usual continuum transport equations for a weakly ionized gas. In spite of these complications, a few observations lead to some important simplying assumptions, and a relatively simple theory can be developed to describe the essential features of the plasmatron.

Transport Equations

The plasmatron is characterized by low plasma electron temperatures. The main plasma electron population is not heated by acceleration through a sheath into the plasma as in the usual arc mode (ignited mode) converter. It enters the

plasma through a small retarding sheath, and has a temperature about equal to the emitter (1400-1600°K). Because of this relatively low electron temperature, account of both electron-ion and electron-neutral collisions must be included in the interelectrode plasma description. It is assumed that electron-electron and electron-ion scattering randomize the direction of the electrons from the emitter, even when this is not accomplished by electron-neutral scattering.

A convenient form of the plasma transport equations which includes electron scattering by both ions and neutrals has been derived by G. Ecker[7] using a constant-collision-frequency approximation. If electron and ion temperatures are assumed to be uniform and the geometry assumed to be one dimensional, these take the form

$$\frac{\Gamma_e}{\mu_e} + \rho_i e n(\Gamma_e - \Gamma_p) = n\frac{dV}{dx} - \frac{kT_e}{e}\frac{dn}{dx}, \tag{1}$$

$$\frac{\Gamma_p}{\mu_p} - \rho_i e n(\Gamma_e - \Gamma_p) = -n\frac{dV}{dx} - \frac{kT_p}{e}\frac{dn}{dx}. \tag{2}$$

where Γ_e and Γ_p are the electron and ion fluxes, μ_e and μ_p the electron and ion mobilities, n the plasma density, V the plasma potential, and T_e and T_p the electron and ion temperatures. The quantity ρ_i is the plasma resistivity due to electron-ion interactions[8]

$$\rho_i = 6.53 \times 10^3 \frac{\ln\Lambda}{T_e^{3/2}} \ \Omega\text{cm}, \tag{3}$$

where T_e is given in degrees Kelvin. The quantity $\ln\Lambda$ is related to the number of particles in a Debye sphere. It is a slow function of plasma density and temperature. Some representative values are shown in Table 1[9].

The addition of equations (1) and (2) eliminates the potential gradient and gives a differential equation for the plasma density distribution:

$$\frac{dn}{dx} = -\frac{e}{k(T_e + T_p)}\left(\frac{\Gamma_e}{\mu_e} + \frac{\Gamma_p}{\mu_p}\right). \tag{4}$$

Ionization in the plasmatron is produced by injected high energy electrons. If it is assumed that this ionization is produced uniformly in the interelectrode space, then, because of current continuity,

Electron density, cm^3	Temperature, °K									
	50	10^2	5×10^2	10^3	5×10^3	10^4	5×10^4	10^5	5×10^5	10^6
10^4	10.69	11.73	14.14	15.18	17.60	18.63	21.05	22.09	24.42	25.11
10^5	9.54	10.58	12.99	14.03	16.44	17.48	19.88	20.94	23.26	23.96
10^6	8.39	9.42	11.84	12.88	15.29	16.33	18.75	19.79	22.11	22.81
10^7	7.23	8.27	10.69	11.73	14.14	15.18	17.60	18.63	20.96	21.65
10^8	6.08	7.12	9.54	10.58	12.99	14.03	16.44	17.48	19.81	20.50
10^9	4.93	5.97	8.39	9.42	11.84	12.88	15.29	16.33	18.66	19.35
10^{10}		4.82	7.23	8.27	10.69	11.73	14.14	15.18	17.51	18.20
10^{11}			6.08	7.12	9.54	10.58	12.99	14.03	16.36	17.05
10^{12}			4.93	5.97	8.39	9.42	11.84	12.88	15.21	15.90
10^{13}				4.82	7.23	8.27	10.69	11.73	14.06	14.75
10^{14}					6.08	7.12	9.54	10.58	12.90	13.60
10^{15}					4.93	5.97	8.39	9.42	11.75	12.45
10^{16}						4.82	7.23	8.27	10.60	11.30
10^{17}							6.08	7.12	9.45	10.14
10^{18}							4.93	5.97	8.30	8.99

Table I - Values of $\ln\Lambda$

$$\frac{d\Gamma_e}{dx} = \frac{d\Gamma_p}{dx} = S. \tag{5}$$

It is assumed for the present that ion loss by recombination is negligible compared to ion loss by flow to the electrodes Using equations (5), equation (4) can be written without the particle fluxes

$$\frac{d^2n}{dx^2} + \frac{S}{D_a} = 0, \tag{6}$$

where D_a, the ambipolar diffusion coefficient, is given by

$$\frac{1}{D_a} = \frac{e}{k(T_e + T_p)} \left(\frac{1}{\mu_e} + \frac{1}{\mu_p}\right). \tag{7}$$

The density distribution in the converter is therefore a quadratic in x where x is the distance from the emitter:

$$n = \alpha_o + \alpha_1 + \frac{\alpha_2}{2} x^2. \tag{8}$$

The coefficients are given by

$$\alpha_o = n_E, \tag{9}$$

$$\alpha_1 = \left.\frac{dn}{dx}\right|_{x=o} = -\frac{T_e}{T_e + T_p}\left(\frac{\Gamma_{eE}}{D_e} + \frac{T_p}{T_e} \cdot \frac{\Gamma_{pE}}{D_p}\right), \tag{10}$$

$$\alpha_2 = \frac{d^2n}{dx^2} = -\frac{S}{D_a}. \tag{11}$$

The parameters D_e and D_p are the electron and ion diffusion coefficients and are related to the corresponding mobilities by the Einstein relations

$$\frac{D_e}{\mu_e} = \frac{kT_e}{e} \quad \text{and} \quad \frac{D_p}{\mu_p} = \frac{kT_p}{e}, \tag{12}$$

and Γ_{eE} and Γ_{pE} are the electron and ion fluxes in the plasma, near the emitter. From equation (5)

$$\Gamma_e(x) = \Gamma_{eE} + Sx , \tag{13}$$

$$\Gamma_p(x) = \Gamma_{pE} + Sx , \tag{14}$$

and

$$\Gamma_{eC} - \Gamma_{eE} = \Gamma_{pC} - \Gamma_{pE} = Sd , \tag{15}$$

where Γ_{eC} and Γ_{pC} are the electron and ion fluxes in the plasma near the collector. The plasma density distribution and density difference across the plasma are therefore given by

$$n = n_E - \frac{T_e}{T_e + T_p}\left(\frac{\Gamma_{eE}}{D_e} + \frac{T_p}{T_e}\frac{\Gamma_{pE}}{D_p}\right) x - \frac{S}{2D_a} x^2, \tag{16}$$

and

$$n_E - n_C = \frac{T_e}{T_e + T_p}\left(\frac{\Gamma_{eE}}{D_e} + \frac{T_p}{T_e}\frac{\Gamma_{pE}}{D_p}\right) d + \frac{S}{2D_a} d^2. \tag{17}$$

By taking the difference of the transport equations, equations (1) and (2), the density gradient is eliminated and an expression is obtained for the electric field in the interelectrode space:

$$\frac{dV}{dx} = \rho e(\Gamma_e - \Gamma_p) + \frac{1}{2n}\left(\frac{\Gamma_e}{\mu_e} - \frac{\Gamma_p}{\mu_p}\right). \tag{18}$$

The potential drop across the plasma V_p is therefore given by

$$-V_p = \rho_i e d(\Gamma_{eC} - \Gamma_{pC}) + \frac{1}{2}\left(\frac{\Gamma_{eE}}{\mu_e} - \frac{\Gamma_{pE}}{\mu_p}\right)\int_o^d \frac{dx}{n} + \frac{S}{2}\left(\frac{1}{\mu_e} + \frac{1}{\mu_p}\right)\int_o^d \frac{x dx}{n}, \tag{19}$$

which is evaluated using the indefinite integrals

$$\int \frac{dx}{n} = \frac{1}{\sqrt{\alpha_1^2 - 4\alpha_o\alpha_2}} \ln \frac{2\alpha_2 x + \alpha_1 - \sqrt{\alpha_1^2 - 4\alpha_o\alpha_2}}{2\alpha_2 x + \alpha_1 - \sqrt{\alpha_1^2 - 4\alpha_o\alpha_2}} \tag{20a}$$

$$\int \frac{x\,dx}{n} = \frac{1}{2\alpha_2} \ln(\alpha_o + \alpha_1 x + \alpha_2 x^2) - \frac{\alpha_1}{2\alpha_2} \int \frac{dx}{n} . \tag{20b}$$

It can be shown that the alternate forms of the integration are not valid in this case.

Boundary Conditions

Calculation of plasmatron performance characteristics requires that some means be developed to relate interelectrode plasma parameters to electrode parameters, that is to relate plasma densities, temperatures, and particle fluxes to electrode or terminal voltages and currents. An exact analysis relating these parameters is very difficult. The electrode-sheath-plasma transition region involves non-equilibrium phenomena and severe anisotropies in the particle distribution functions -- even the actual thickness of this region is not known before hand. Fortunately, a detailed analysis of this transition region is not necessary. The thickness of the region is the order of a Debye length, very small compared to the interelectrode space. Therefore, to a first approximation, it can be assumed that the sheaths have zero thickness. The first order effect of the sheaths is to control the particle fluxes at the plasma-electrode boundary. A simple statement of particle conservation describes this role of the sheaths and thus provides approximate boundary conditions for a solution of the plasma problem. The particles near the boundaries have nearly a Maxwellian distribution in energy. There are some anisotropies in these distributions, but these can be corrected with a simple P_1 approximation. That is, the forward and backward random fluxes for the electrons can be approximated by

$$\Gamma_+ = \frac{nv_e}{4} + \frac{\Gamma_e}{2} , \tag{21}$$

$$\Gamma_- = \frac{nv_e}{4} - \frac{\Gamma_e}{2} . \tag{22}$$

so that the total net electron flux is given by

$$\Gamma_+ - \Gamma_- = \Gamma_e. \tag{23}$$

The ion fluxes can be described in a similar way. This approximation is used here to generate the desired boundary conditions.

In the plasmatron we are not ordinarily interested in the inefficient case of excess ion generation, that is, of space charge overcompensation. Thus, the emitter is assumed to have a negative sheath as shown in Fig. 7,

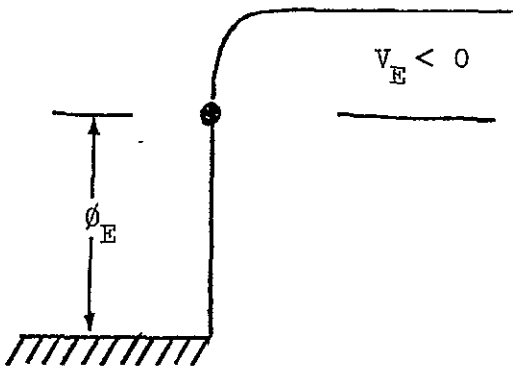

Fig. 7 Motive Diagram at the Emitter

where V_E is the emitter sheath potential and ϕ_E the emitter work function. The boundary conditions at the emitter for this case are given by[10]

$$\nu_e \exp\left(\frac{eV_E}{kT_{eE}}\right) - \left(\frac{n_E v_{eE}}{4}, \frac{\Gamma_{eE}}{2}\right) = \Gamma_{eE}, \tag{24}$$

$$-\left(\frac{n_E v_{pE}}{4} - \frac{\Gamma_{pE}}{2}\right) \exp\left(\frac{eV_E}{kT_{pE}}\right) + \nu_p = \Gamma_{pE}, \tag{25}$$

where ν_e and ν_p are the saturation electron and ion emission from the emitter, T_{eE} and T_{pE} the electron and ion temperature near the emitter, n_E the plasma density near the emitter, v_{eE} and v_{pE} the mean electron and ion velocities near the emitter, and Γ_{CE} and Γ_{pE} the plasma electron and ion fluxes near the emitter.

A reasonable assumption here is that both electrons and ions near the emitter are at the emitter temperature

$$T_{eE} = T_{eC} = T_E \tag{26}$$

A more severe assumption, one nevertheless made for this analysis, is that the electron temperature in the converter (except for the fast electrons from the auxiliary electrode) is uniform.

$$T_e \approx T_E. \tag{27}$$

Actually there should be some heating of the main conduction electrons because of the plasma drop and because of interaction with the fast, ionizing electrons. Also, there should be some cooling of these electrons because of radiation, and particularly at the collector, because of the transport of electron kinetic energy out of the plasma to the collector. For this preliminary analysis, these latter effects are ignored, but they deserve further investigation in view of their potential importance. The ion temperature is another matter. For higher pressures, where the ratio of spacing to electron-mean free path is large, one would expect the ion temperature to be in local equilibrium with the neutral gas and to vary linearly from the emitter to the collector. For the case of most interest, where the spacing is about equal to the mean free path, the ions will be generated from two atom streams, one coming from the emitter, the other from the collector. Those reaching the collector will come mainly from the emitter. Therefore, in this preliminary study it is assumed that the ions also have a uniform temperature equal to the emitter temperature

$$T_p \approx T_E \tag{28}$$

Whatever the uniform temperatures, the electron and ion velocities are given by

$$v_e = \sqrt{\frac{8k\,T_e}{\pi m}}, \tag{29}$$

$$v_p = \sqrt{\frac{8k\,T_p}{\pi M}}. \tag{30}$$

where m and M are the electron and ion masses.

To obtain the full volt-ampere characteristic, boundary conditions for two cases are needed for the collector. The collector sheath may be positive or negative depending on the voltage output of the converter. For a positive sheath[10],

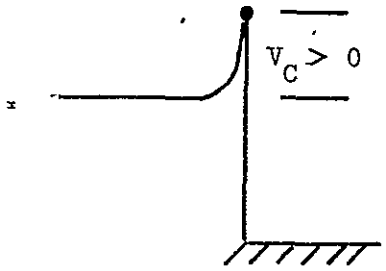

$$\left\{ \left(\frac{n_C v_e}{4} + \frac{\Gamma_{eC}}{2} \right) \exp\left(- \frac{eV_C}{kT_e} \right) = \Gamma_{eC} \right. \tag{31}$$

$$\left. \frac{n_C v_p}{4} = \frac{\Gamma_{pC}}{2} , \right. \tag{32}$$

and for a negative sheath[10],

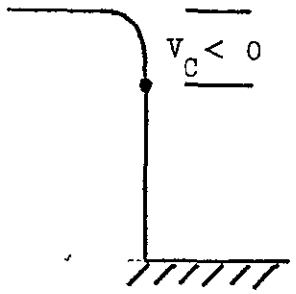

$$\left\{ \frac{n_C v_e}{4} = \frac{\Gamma_{eC}}{2} , \right. \tag{33}$$

$$\left. \left(\frac{n_C v_p}{4} + \frac{\Gamma_{pC}}{2} \right) \exp\left(\frac{eV_C}{kT_p} \right) = \Gamma_{pC} , \right. \tag{34}$$

where n_C is the plasma density near the collector and Γ_{eC} and Γ_{pC} are the electron and ion fluxes near the collector. These boundary conditions can be put into more useful form if we define the variables R and Q.

$$R = \frac{D_e}{D_p} \frac{\Gamma_{pE}}{\Gamma_{eE}} \tag{35}$$

This is equivalent to the R variable used in the theory of the unignited mode[10], to which the plasmatron reduces if the fluxes to and from the auxiliary electrode become zero. The variable Q is dependent on the ion generation rate

$$Q = \frac{\Gamma_{eC}}{\Gamma_{eE}} \cdot \frac{\Gamma_{pE}}{\Gamma_{pC}} = \left(1 + \frac{Sd}{\Gamma_{eE}} \right) \Big/ \left(1 + \frac{Sd}{\Gamma_{pE}} \right) \tag{36}$$

We also introduce the variable

$$\beta_E = \frac{\nu_p}{\nu_e}\frac{v_e}{v_p} = \frac{\nu_p}{\nu_e}\sqrt{\frac{M}{m}}, \tag{37}$$

the ion-richness emission ratio for the emitter. The collector boundary conditions can now be simplified. Equations (33) and (34) combine to give

$$\exp\left(-\frac{eV_C}{kT_p}\right) = \frac{1}{2}\left(\frac{\lambda_e Q}{\lambda_p R} + 1\right) \qquad V_C \leq 0 \tag{38}$$

and equations (31) and (32) combine to give

$$\exp\left(\frac{eV_C}{kT_e}\right) = \frac{1}{2}\left(\frac{\lambda_p R}{\lambda_e Q} + 1\right) \qquad V_C \geq 0 \tag{39}$$

Note that the full volt-ampere characteristic ($-\infty < V_C < \infty$) corresponds to the variable R/Q moving through the range 0 to ∞.

Plasmatron Solution

The emitter electron boundary condition, equation (24), can be written

$$\exp\left(\frac{eV_E}{kT_E}\right) = \frac{n_E v_e}{4\nu_e} + \frac{\Gamma_{eE}}{2\nu_e}. \tag{40}$$

Substituting equations (15), (17), and (33), this becomes

$$\exp\left(\frac{eV_E}{kT_E}\right) = \frac{\Gamma_{eC}}{\nu_e}\{1 + \Delta\} - \xi, \qquad V_C \leq 0 \tag{41}$$

where

$$\Delta = \frac{T_e}{T_e + T_p}\left(1 + \frac{T_p}{T_e}\frac{R}{Q}\right)\frac{3d}{4\lambda_e}, \tag{42}$$

$$\xi = \frac{Sd}{\nu_e}\left[\frac{1}{2} + \frac{T_e}{T_e + T_p}\left(1 + \frac{T_p}{T_e}\frac{D_e}{D_p}\right)\frac{3d}{4\lambda_e} - \frac{3d}{8\lambda_a}\cdot\frac{v_e}{v_p}\right], \qquad (43)$$

where
$$\lambda_a = \frac{3D_a}{v_p}. \qquad (44)$$

The latter is an equivalent ion mean free path corresponding to the ambipolar diffusion coefficient D_a.

If equation (41) is now substituted into equation (25), and the approximation $T_p = T_E$ accepted, the emitter sheath potential can be eliminated, giving a quadratic in the electron flux at the collector

$$Aw^2 + Bw + C = 0, \qquad (45)$$

where
$$w = \frac{\Gamma_{eC}}{\nu_e}, \qquad (46)$$

$$A = -\frac{R}{Q}\frac{\lambda_p}{\lambda_e}\frac{1}{2}(1+\Delta) + (\frac{1}{2}+\Delta)(1+\Delta), \qquad (47)$$

$$B = \frac{1}{2}\frac{Sd}{\nu_e}(1+\Delta)\frac{v_e}{v_p} + \frac{R}{Q}\frac{\lambda_p}{\lambda_e}(1+\frac{\xi}{2}) - \xi(\frac{1}{2}+\Delta) + (1+\Delta)\left(\frac{Sd}{2\nu_e} - \xi\right), \qquad (48)$$

$$C = \beta_E - \frac{Sd}{\nu_e}\frac{v_e}{v_p}(1+\frac{\xi}{2}) - \xi\left(\frac{Sd}{2\nu_e} - \xi\right). \qquad (49)$$

This result has been derived using equation (33), and therefore, equation (41) and the subsequent equations (45-49) apply only to the case $V_C \leq 0$. Using equation (32) instead of (33), equation (41) becomes

$$\exp\left(\frac{eV_E}{kT_E}\right) = \frac{\Gamma_{eC}}{\nu_e}(1+\Delta') - \xi, \qquad V_C \geq 0 \qquad (50)$$

where $$\Delta' = \Delta - \frac{1}{2}\left(1 - \frac{\lambda_p}{\lambda_e}\,\frac{R}{Q}\right). \qquad (51)$$

The solution written as equations (45-49) is still valid, therefore, if Δ is reinterpreted according to equation (51).

Calculation Procedure

A volt-ampere characteristic for the plasmatron can be calculated if values are specified for the following variables:

T_E = emitter temperature

T_C = collector temperature

ϕ_E or $J_R(E)$ = emitter work function or Richardson emission at the emitter

T_R = reservoir temperature (for cesium)

P = gas pressure (for argon)

$I(A)$ = auxiliary electrode current

V_B = auxiliary electrode bias

ϕ_C = collector work function

d = spacing

V_i = ionization potential

$\sqrt{\frac{M}{m}}$ = root of the atom to electron mass ratio

P_C = electron-atom elastic collision probability

μ_o = ion mobility coefficient

A particular position on the volt-ampere curve is characterized by a value for the variable R/Q. To plot out a complete volt-ampere curve in the present calculation program R/Q was first given the value 10^{-5} and then increased by repetitive factors of two until the value 10^{3} was exceeded. For a given value of R/Q, the following calculational sequence was followed:

1. Whichever variable ϕ_E or $J_R(E)$ is not given is calculated from the Richardson equation

$$J_R(E) = 120\, T_E^{\,2} \exp(-\phi_E/kT_E), \qquad (52)$$

$$\phi_E = -kT_E \ln \frac{J_R(E)}{120\ T_E^2} . \tag{53}$$

2. The ionization probability for the emitter surface is calculated.

$$\beta^* = \left[1 + 2 \exp\left(\frac{V_i - \phi_E}{kT_E}\right)\right]^{-1} . \tag{54}$$

3. The emitter ion emission rate is calculated.

$$\nu_p = \mu_a \beta^* . \tag{55}$$

where μ_a is the heavy particle arrival rate. For cesium,

$$\mu_a \approx 10^{27} \exp\left(\frac{-.75}{kT_R}\right) . \tag{56}$$

4. The electron and ion velocities are calculated.

$$v_e = 1.96 \times 10^7 \sqrt{\frac{T_E}{10^3}} \tag{57}$$

$$v_p = v_e \sqrt{\frac{m}{M}} . \tag{58}$$

5. The emitter ion emission richness ratio is calculated.

$$\beta_E = \frac{\nu_p}{\nu_e} \frac{v_e}{v_p} \tag{59}$$

6. The mean free path is calculated.

$$\lambda_e = \frac{1}{P_C} \frac{T_E}{273} \frac{1}{P} . \tag{60}$$

where P_C is the collision frequency[11]

$$P_C \text{ (cesium)} \doteq 1000$$

$$P_C \text{ (argon)} = 6$$

and P is the gas pressure. For cesium

$$P = 2.45 \times 10^{8} \frac{1}{\sqrt{T_R}} \exp\left(-\frac{8910}{T_R}\right). \tag{61}$$

7. The diffusion coefficient $D_e = \frac{\lambda_e v_e}{3}$ is calculated.

8. Atom density, using the ideal gas law is calculated,

$$N_a = P \cdot 1333/kT_E. \tag{62}$$

where here $k = 1.38 \times 10^{-16}$ erg $^{o}C^{-1}$.

9. The ion mobility is calculated.[11]

$$\mu_p = \mu_o \times \frac{2.69 \times 10^{19}}{N_a} \sqrt{\frac{600}{T_E}}. \tag{63}$$

For cesium $\mu_o = .07$,

for argon $\mu_o = 1.6$

10. The ion mean free path is calculated.

$$\lambda_p = \frac{3\mu_p}{v_p} \frac{kT_p}{e}. \tag{64}$$

11. Using the relative bias $x = V_B/V_i$, the ionization cross section is calculated according to the classical formula of Gryzinski[12]

$$\sigma_i = \frac{6.56 \times 10^{-14}}{V_i^2} \cdot \frac{1}{x} \left(\frac{x-1}{x+1}\right)^{3/2} \left\{1 + \frac{2}{3}\left(1 - \frac{1}{2x}\right) \ln\left[e + (x-1)^{\frac{1}{2}}\right]\right\}. \tag{65}$$

12. Using this cross section the strength of the ion source is calculated.

$$Sd = \frac{I(A)\, N_a \sigma_i d}{2e} \tag{66}$$

13. The equivalent ambipolar mean free path is calculated.

$$\lambda_a = \frac{3D_a}{v_p}, \tag{67}$$

where D_a is given by equation (7)

$$\frac{1}{D_a} = \frac{e}{k(T_e + T_p)} \left(\frac{1}{\mu_e} + \frac{1}{\mu_p}\right), \tag{68}$$

and

$$\frac{1}{\mu_e} = \frac{kT_E}{e} \cdot \frac{1}{D_e}. \tag{69}$$

14. ξ is calculated using equation (43).

15. Δ, Δ' is calculated using equations (42) or (51).

16. A, B, and C are calculated using equations (47-49).

17. w (equation 45) is solved with the quadratic formula.

18. Γ_{pC} is solved for

$$\frac{\Gamma_{pc}}{\nu_e} = \frac{\Gamma_{ec}}{\nu_e} \cdot \frac{R}{Q} \cdot \frac{D_p}{D_e}. \tag{70}$$

19. The output current is obtained

$$\frac{J}{e\nu_e} = \frac{\Gamma_{eE} - \Gamma_{pE}}{\nu_e}. \tag{71}$$

20. The collector sheath potential V_C is calculated using equations (38 or 39).

21. The plasma drop V_p is calculated using equation (20).

22. The emitter sheath potential is calculated using equation (41).

23. The converter voltage drop is calculated.

$$V_d = V_E - V_p - V_C. \tag{72}$$

24. The converter output voltage is calculated.

$$V_o = \phi_E - \phi_C - V_d. \tag{73}$$

25. The pair J - V_o is plotted, and the computation is repeated with R/Q multiplied by a factor of two.

Computer Program

Theoretical current-voltage characteristics were calculated and plotted on a Hewlett-Packard 9820A Calculator and 9862A plotter. The register definitions and computer program are as follows.

A = A
B = B
C = C
X = V_o
Y = $J/e\nu_e$
R(1) = ϕ_E
R(2) = T_E
R(3) = $J_R(E)$
R(4) = I(A)
R(5) = V_B
R(6) = T_R
R(7) = ϕ_C
R(8) = d
R(9) = $\sqrt{M/m}$
R(10) = V_i
R(11) = σ_o
R(12) = R/Q
R(13) = ν_e
R(14) = β^*
R(15) = ν_p
R(16) = v_e
R(17) = v_p
R(18) = β_E
R(19) = P
R(20) = λ_e
R(21) = D_e
R(22) = N_a
R(23) = μ_p
R(24) = λ_p
R(25) = x
R(26) = σ
R(27) = Sd
R(28) = D_a
R(31) = λ_a
R(32) = ξ
R(33) = Γ_{eC}/ν_e
R(34) = Γ_{eE}
R(35) = Γ_{pC}/ν_e
R(36) = Γ_{pE}
R(37) = $\lambda_p R/D_e Q$
R(38) = eV_C/kT_E
R(39) = eV_E/kT_E
R(40) = D_p
R(41) = μ_e
R(42) = part of R(26)
R(43) = T_C
R(44) = T_p
R(45) = part of R(39)
R(46) = eV_p/kT_E
R(47) = eV_d/kT_E
R(48) = α_o
R(49) = α_1
R(50) = α_2
R(51) = Δ, Δ'
R(52) = ρ_i
R(53) = $\int \frac{dx}{n}$
R(54) = $\int \frac{x dx}{n}$
R(55) = $\sqrt{\alpha_1^2 - 4\alpha_o\alpha_2}$

```
0:
⊢
1:
ENT "PHI(E)";R1,
"TE",R2,"JR",R3,
"I(A)",R4,"VBIAS
";R5⊢
2:
ENT "PHI(C)",R7,
"TC",R43,"D",P8,
"VI",P10⊢
3:
ENT "ΓMI/ME",R57
,"PC",P11,"MU 0"
,P45,"P(A)",R19⊢
4:
ENT "JMAX",P56,"
VMIN",P42,"VMAX"
,P30⊢
5:
(P2+P43( 2→P44:P
57Γ(R2/P44)→P9⊢
6:
120R2P2÷EXP (-P1
 (8.62E-5÷R2))→P
3⊢
7:
P3 1.6E-19→P13⊢
8:
1.96E7-Γ(P2. 1000
)→R16⊢
9:
R16 P9→P17⊢
10:
P2 273 R19. P11→P
20:-R8 2. P20→P6⊢
11:
P20R16 3→R21⊢
12:
P19÷1333. (1.38E-
16→P2)→P22⊢
13:
R45÷2.69E19÷Γ(60
0 P21. P22→R23⊢
14:
3P23÷8.62E-5÷P44
. P17→P24⊢
15:
R5 R10→P25⊢
16:
Γ 50E-14. P10R10R
25÷((P25-1)/(R25
+1)((1)3 2)→R26⊢
17:
P26(1+2)1-1/2P25
)LN (2.7183+Γ(R2
5-1)(1/3)→P26⊢
18:
P26R22R4R8(1-
E^P R6)/-R6 2, 1.
6E-19→P27⊢
19:
P21/8.62E-5/P2→P
41⊢
20:
P24→P17, 3→P40⊢
21:
3-(P23→P21+P40→P
41: P17 (P23+R41
)→R31⊢
22:
6.5E3→P21(-3 2)→
LN 10→R52⊢
23:
1E-5→P12:GSB "FL
G"⊢
24:
IF P39 0:DSP "NE
 0":STP ⊢
25:
FIX 3:PRT "I(A)
(P)=",P4,"JP (A/
CM2)=",P3⊢
26:
PRT "JSAT (A/CM2
)=",Y,"VMIN (VOL
T)=",X,"IA/JSAT"
,P4 Y:IF FLG 0:
GTO +19⊢
27:
IF R56≠0:GTO +2⊢
28:
ENT "JMAX",P56,"
VMIN",P42,"VMAX"
,P30⊢
29:
SCL P42-.1,P30+.
2,-P56 10,1.1P56
⊢
```

```
30:
AXE 0,0,.25,R56
10┘
31:
P42→P29:END 1┘
32:
LTP R29,-R56 20,
211┘
33:
PLT P29┘
34:
JMP 3(1P29+.5→R2
9)`P30)-2┘
35:
IF P56≥.01:END 4
:GTO +2┘
36:
END 2┘
37:
0→P29┘
38:
LTP -.25,P29,211
┘
39:
PLT P29┘
40:
JMP 3)1P29+P56.5
→P29) P56)-2┘
41:
LTP )P20+P42) 2,
-P56`10,321┘
42:
PLT "V )VOLT)"┘
43:
LTR .05,P56,321┘
44:
PLT "J )A CM2)"┘
45:
LTP X,Y→P56 50,2
11┘
46:
PLT 'I)A) )A CM2
="┘
47:
LTP X+P30 2.5,Y+
P56 50,211┘
48:
END 4:PLT P4:
PLT ┘
```

```
49:
GSB "FLG"┘
50:
PLT X,Y┘
51:
2P12→P12:IF R12<
1E3:GTO -2┘
52:
GTO "END"┘
53:
"FLG"┘
54:
.5+P211+P44P21 P
2P40)3P8`4P20)P2
+P44)→P32┘
55:
P27)P32-3P8R16 8
P31P17) P13→P32┘
56:
P24P12.P20→P37┘
57:
3P2P8)1+P44P12 P
21`4P20)P2+R44)→
P54┘
58:
IF P37=1:GTO +2┘
59:
R51-.5)1-P37)→R5
1┘
60:
-.5P37)1+P51)+),
5+P51)1+P51)→A┘
61:
.5P27)1+P51)P16
P17P13+P37)1+P32
.2)-P32).5+R51)→
B┘
62:
B+(1+R51))P27 2P
13-P32)→B┘
63:
-P18-P27)1+P32.2
:P16 R13P17-P32)
P27 2P13-P32)→C┘
64:
(-B`2 A)↑2-(-B)
-B`2 A→P33┘
```

```
65:
P33R12P40/P21→R3
5⊢
66:
(R33-R35)→R13*1.
602E-19→Y⊢
67:
P33P13-P27→P34:P
35P13-P27→P36⊢
68:
IF P37 1:GTO +2⊢
69:
-LN (1 R37+1) 2
)→P38:GTO +2⊢
70:
LN (1+P37) 21→P
38⊢
71:
-P2)P34 P21→P44P
36·P2P40) (P2→P4
4)→P49⊢
72:
P31P17 3→P28⊢
73:
-P27 3P8P28→P50⊢
74:
IF R37-1:GTO +2⊢
75:
3P35P13 P17-P49P
8-P50P8P8→P48:
GTO +2⊢
76:
3P33P13 P16-P49P
8-P50P8P8→P48⊢
77:
IF P4≠0:GTO +3⊢
78:
LN (P49P8 P48+1)
P49→P53⊢
79:
P8 P49-P48LN (P4
9P9·P48÷1) P49P4
9→P54:GTO +7⊢
80:
5)P49↑2-4P48P50)
→P55⊢
81:
(R49-R55)) (R842P
50+P8P49+P48)→P5
3⊢
82:
2LN ((R48+(2P8P5
0+P49-P55)·P53)·
P55→P53⊢
83:
(P49-P55)(2P50P8
+P49+P55)→R54⊢
84:
R49LN ((R49+P55)
(2P50P8+P49-P55)
P54)·2P50P55→P5
9⊢
85:
LN (P8↑2P50 P48+
P8P49 P48+1) 2P5
0→P54→P54⊢
86:
1.602E-19→P8P52P
13)P35-P33)÷.5)P
26 P23-P34.P41)P
53→P46⊢
87:
P46÷.5P27)) P23-
1 P41:P54 P8→P46
⊢
88:
LN (P33)) (P51)→P
32)→P39⊢
89:
P39-P46 (8.62E-5
→P2)→P38→P47⊢
90:
P1→P7-8.62E-5→P2
→P47→Y⊢
91:
PET ⊢
92:
"END":END ⊢
P77
```

V. EXPERIMENTAL AND ANALYTICAL RESULTS

Examples of typical experimental I-V characteristics for the plasmatron are shown in Fig. 8. Also shown are some corresponding theoretical characteristics obtained using the computer program of the previous chapter. As the figure shows, the theory follows the experimental trends fairly well. The theory is useful, therefore, to assist in the interpretation of the experimental data.

Current Amplification

One means of judging plasmatron performance is the effectiveness of output current enhancement by the auxiliary discharge current. This can be expressed in terms of a current amplification factor A which is the ratio of converter current to auxiliary electrode current

$$A = \frac{I}{I_A} \tag{74}$$

The significance of this factor is most evident if an equivalent arc drop V_d^* is also defined. The latter is convenient for performance comparison to the arc mode (ignited mode) diode converter. The equivalent arc drop V_d^* is defined for the plasmatron as the auxiliary power consumed to produce a given output current I divided by that current itself

$$V_d^* = \frac{\text{auxiliary power}}{\text{output current}} = \frac{I_A V_B}{I} = \frac{V_B}{A} . \tag{75}$$

The auxiliary electrode bias potential V_B is somewhat larger than the ionization potential of the gas. It is evident from equation (75) that, for best performance, the plasmatron should use a gas with a low ionization potential (to be able to use a low bias) and with a large amplification factor. Unless the resulting equivalent arc drop V_d^* is much less than the ignited mode arc drop (≈ 0.5 volts) there is little motivation to add the complication of the auxiliary electrode.

Actual internal voltage drops in the device which tend to move the I-V characteristic out of the power quadrant, are also important and should be evaluated. It can be seen in Fig. 8, for example, that the saturation (maximum current) region occurs out of the power quadrant. The reason for this needs to be determined so it can be decided if this is an inherent limitation of the plasmatron.

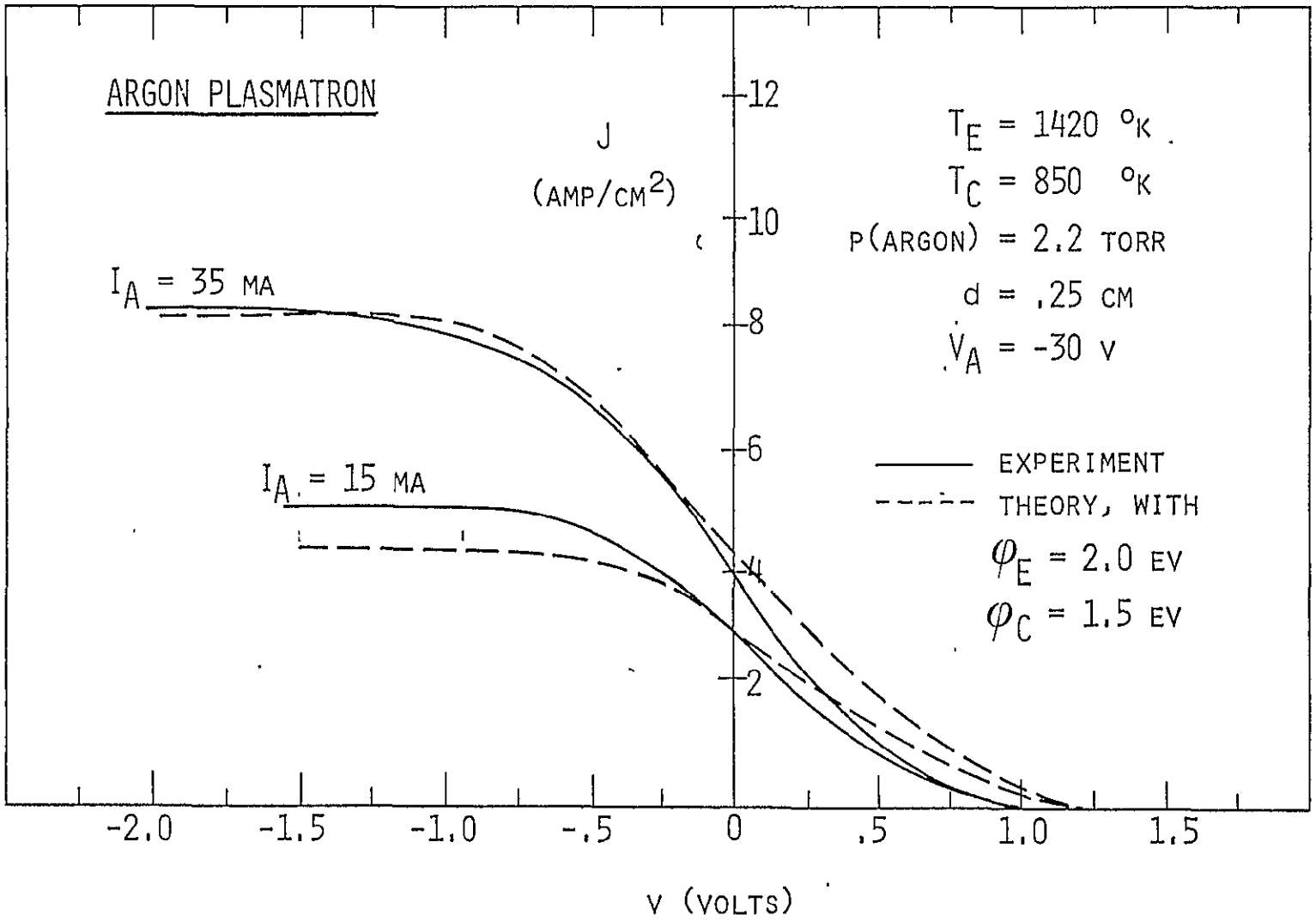

Fig. 8 Theoretical and Experimental I-V Characteristics for an Argon Plasmatron

The saturation output current I_S versus auxiliary current for the cesium and argon plasmatrons are shown in Figs. 9 and 10. Constant values of amplification factor A appear as converging straight lines in those figures, which also correspond to constant values of equivalent arc drop V_d^*. For the biases given in the figure, the corresponding arc drops are listed for each of the converging lines. As these results show, the converter saturation current versus auxiliary current is represented reasonably well by the computer program. The experimental data however show a drop-off in amplification at high converter currents greater than that found in the calculations. This, for example, could be due to energy relaxation in the ionizing electron beam from the auxiliary electrode. As the converter current increases, the plasma density increases, and accordingly, the relaxation rate for this beam also increases. The beam therefore becomes less efficient in ionizing the argon. Such an effect is not included in the calculations. The effect might also be due to plasma recombination, which also is neglected in the calculations. The cesium plasmatron might be expected, a priori, to have greater amplification factors and lower equivalent arc drops because of the lower mobility of the heavier cesium ions and because of the lower ionization potential for cesium. In practice, however, argon gives significantly better performance. The equivalent arc drop for the cesium plasmatron is no better than the arc drop ($V_d \approx 0.5$ volts) typical for the arc mode diode converter.

Scattering Effects

The superior performance of the argon plasmatron is related to the optimum pressure observed in these devices. Fig. 11 shows an example of this for argon. For a given bias V_A, the amplification A first increases with pressure due to the increase in the density of ionization target atoms. For best performance, at least one ion pair should be produced for each injected electron. Unfortunately, these target atoms can also scatter the low energy élelectrons from the main emitter back to the emitter causing a loss in converter current as pressure increases. This is shown in Fig. 11 by the drop in amplification as pressure continues to increase. The optimum pressure occurs when the low energy electron mean free path is the order of the interelectrode spacing.

With argon this back-scatter limitation does not become serious as ion generation is optimized, because the ionization cross section for argon at the high electron injection energy is greater than the electron-neutral cross section

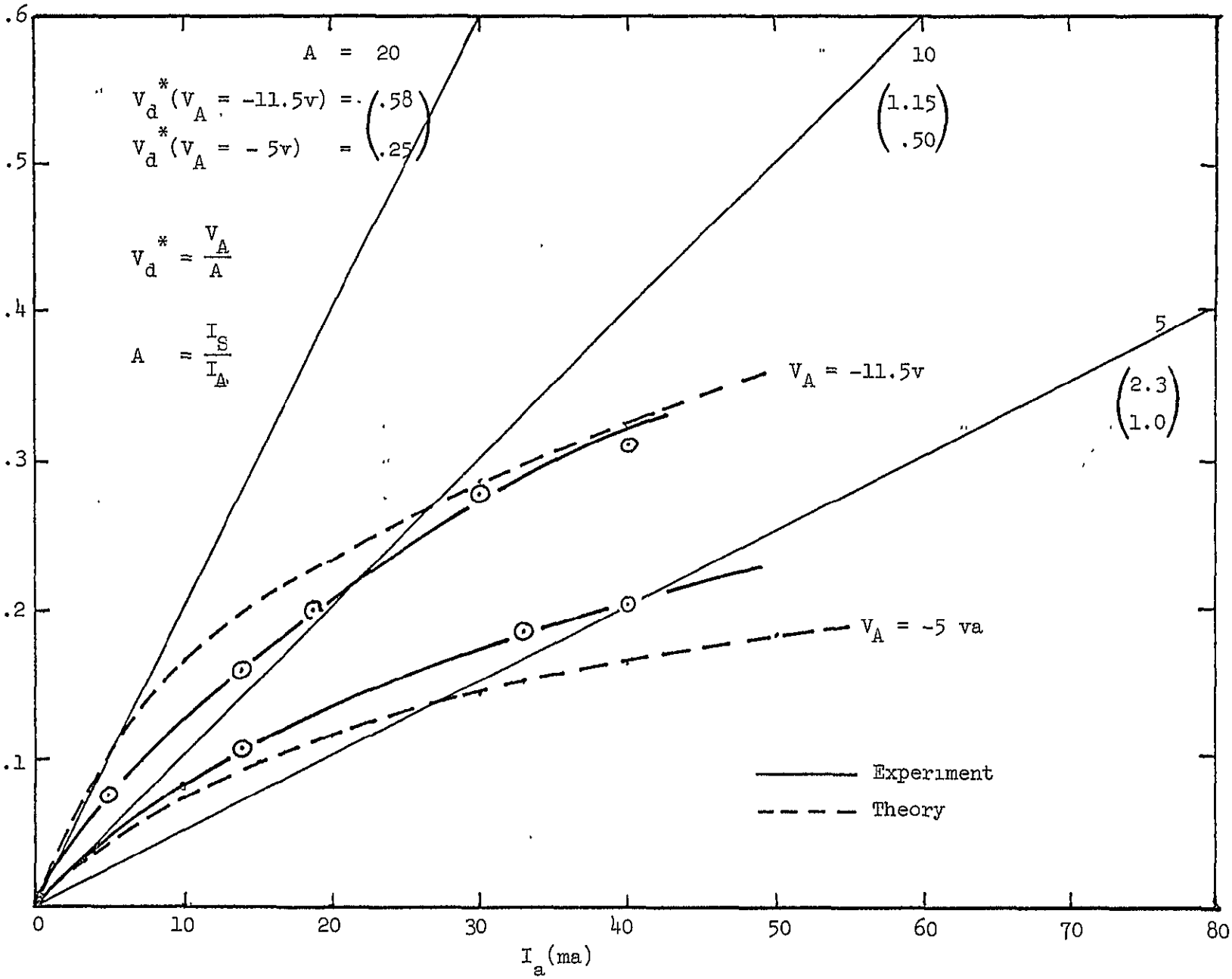

Fig. 9 Experimental and Theoretical Performance of Cesium Plasmatron

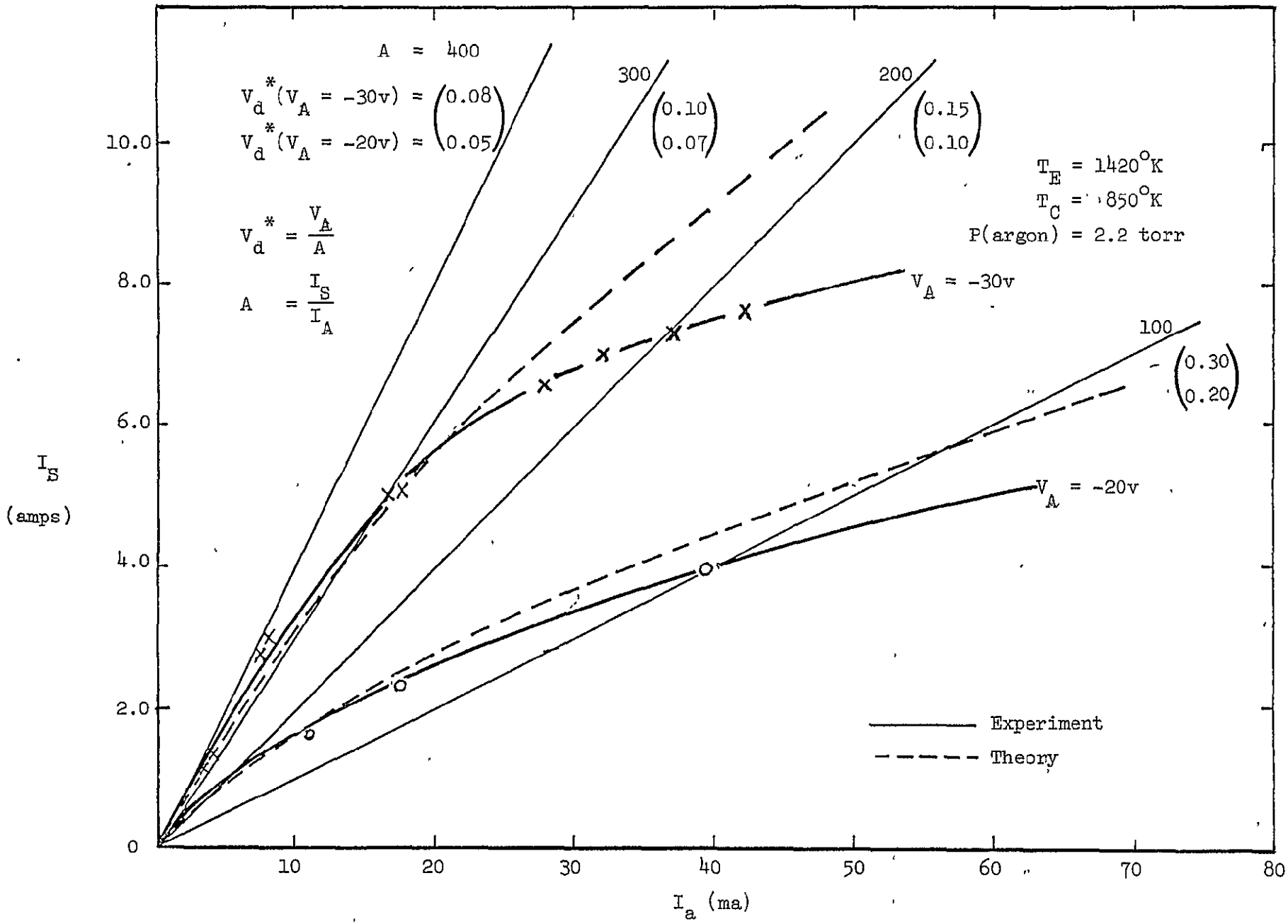

Fig. 10 Experimental and Theoretical Performance of Argon Plasmatron

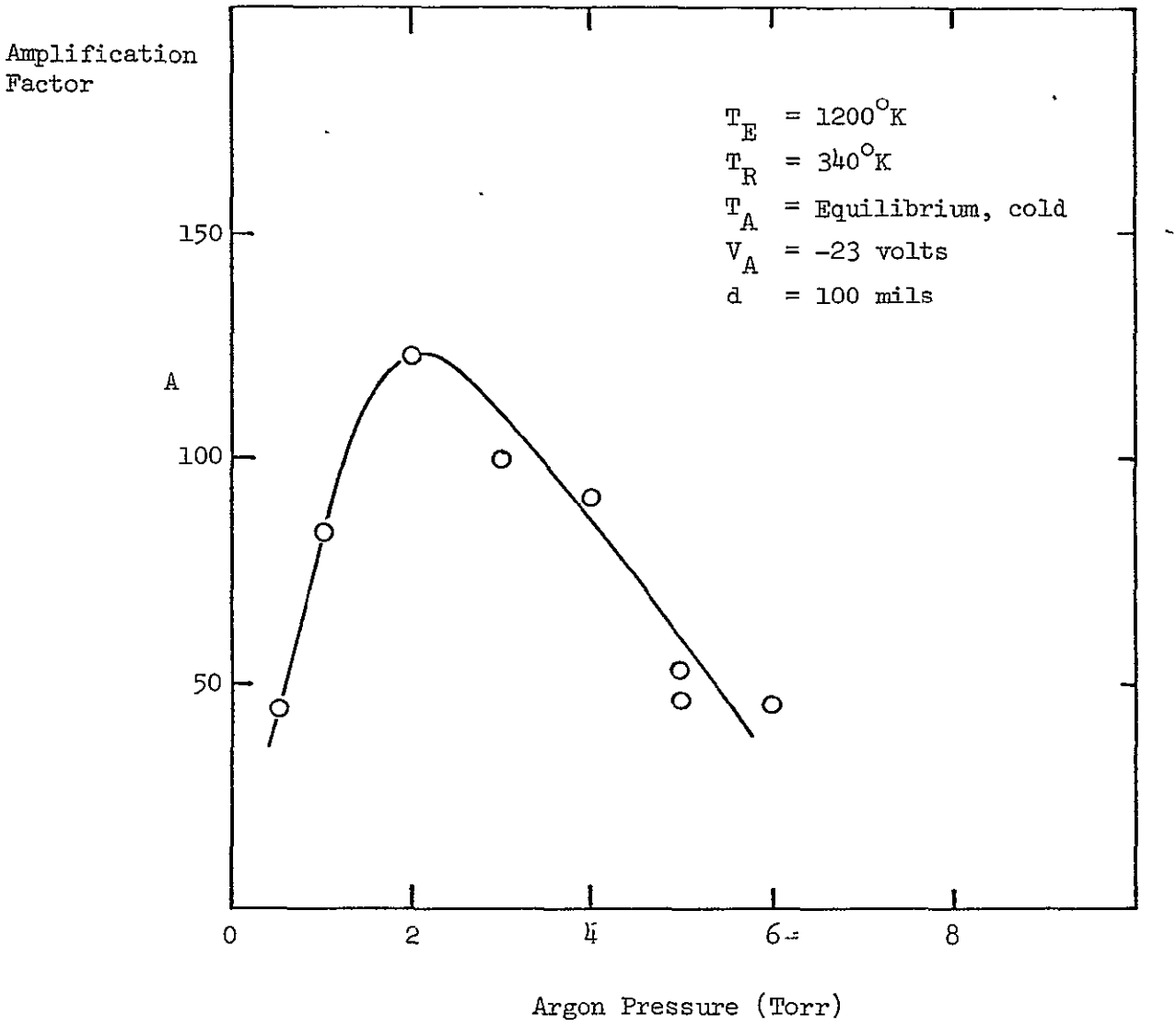

Fig. 11 Amplification Factor as a Function of Argon Pressure

at the lower, plasma-conduction electron energy. These cross sections are shown in Fig. 12 as a function of electron velocity. It should be noted that this advantageous cross section ratio does not occur with cesium. As the cross sections in Fig. 12 show, backscatter becomes important for cesium before the pressure is high enough to optimize ion generation.

A further scattering effect becomes important to plasmatron performance which is not usually important in the arc-mode (ignited-mode) diode, that is, the component of plasma resistivity, ρ_i arising from electron-ion scattering. This is given by

$$\rho_i = 6.5 \times 10^3 \frac{\ln\Lambda}{T_e^{3/2}} \quad \text{ohm-cm}, \tag{76}$$

where T_e is the plasma electron temperature and $\ln\Lambda$ is the order of 3-5. In the optimum ignited-mode diode, plasma electron temperatures can be as high as 3000-4000°K, while in the plasmatron the plasma electron temperatures are relatively low, approximately equal to the emitter temperature (1400-1600°K). Because of the reciprocal dependence of ρ_i on $T_e^{3/2}$ this resistance becomes particularly important in the plasmatron. The effect of this on the current-voltage characteristic can be seen in Fig. 13 where two sets of calculated characteristics are shown, one including the effects of electron-ion collisions ($\rho_i \neq 0$), a second excluding them ($\rho_i = 0$). For large current densities and for the very wide electrode spacing of Fig. 13 (voltage loss due to this resistivity is proportional to both) the voltage loss is serious, actually moving the saturation current well out of the power quadrant. At relatively low current densities and close spacings, however, this loss is reduced and becomes tolerable.

Distribution of Enhanced Output Current

The output current distribution for the plasmatron was measured using the probes mounted in the collectors. A series of I-V curves for these probes in the cylindrical device are shown in Fig. 14. The upper I-V curve in each photo is the total converter output current; the lower (at a different scale factor) is the probe current. The position of the probes for this sequence of I-V characteristics is shown in Fig. 15. Probe 4 is in the plane of the auxiliary electrode. The enhanced current distribution is a function of many effects: the width of the ion generation region, the extent of spreading of the ions along

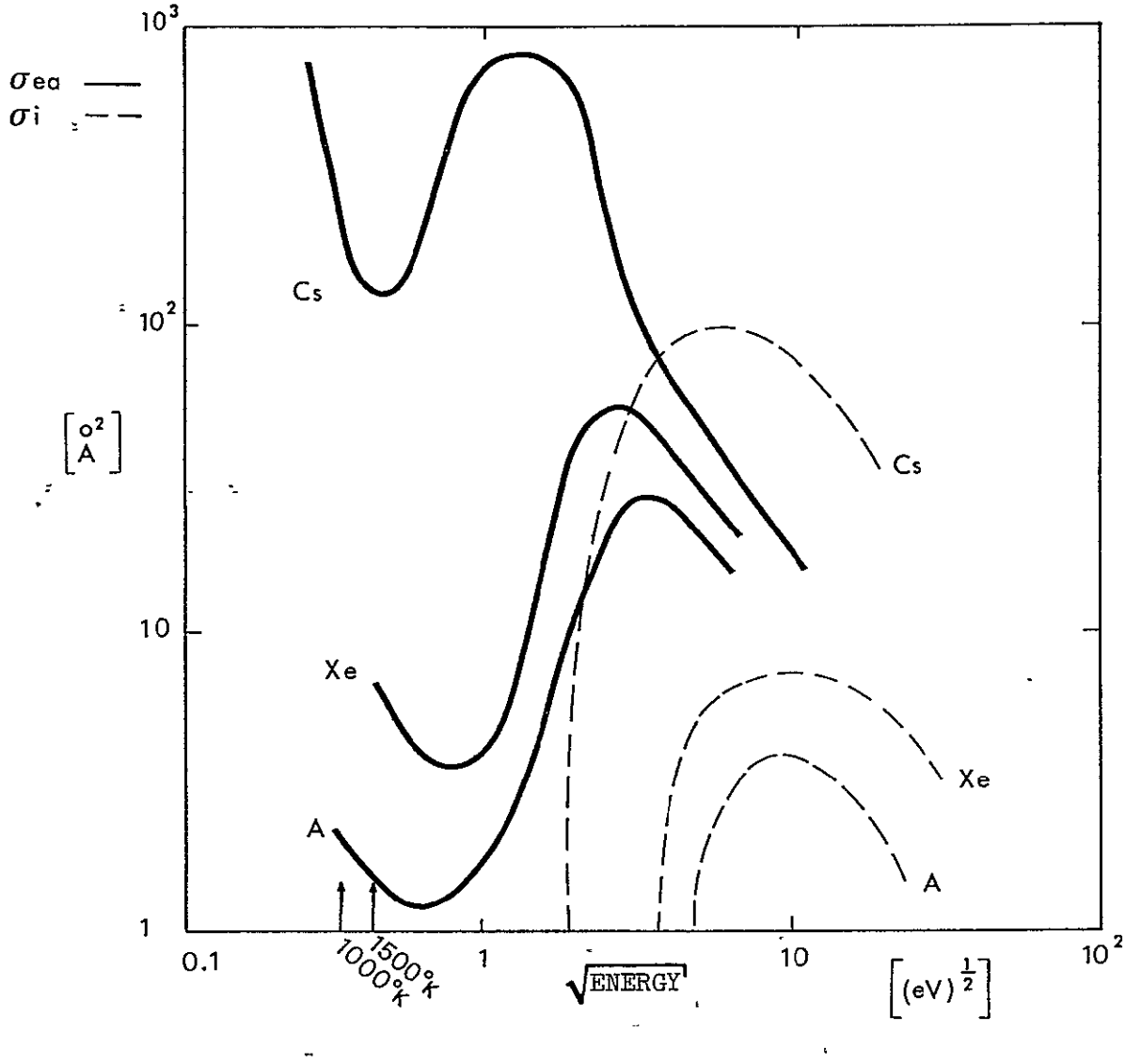

Fig. 12 Electron-Cesium and Electron-Noble Gas Cross Sections

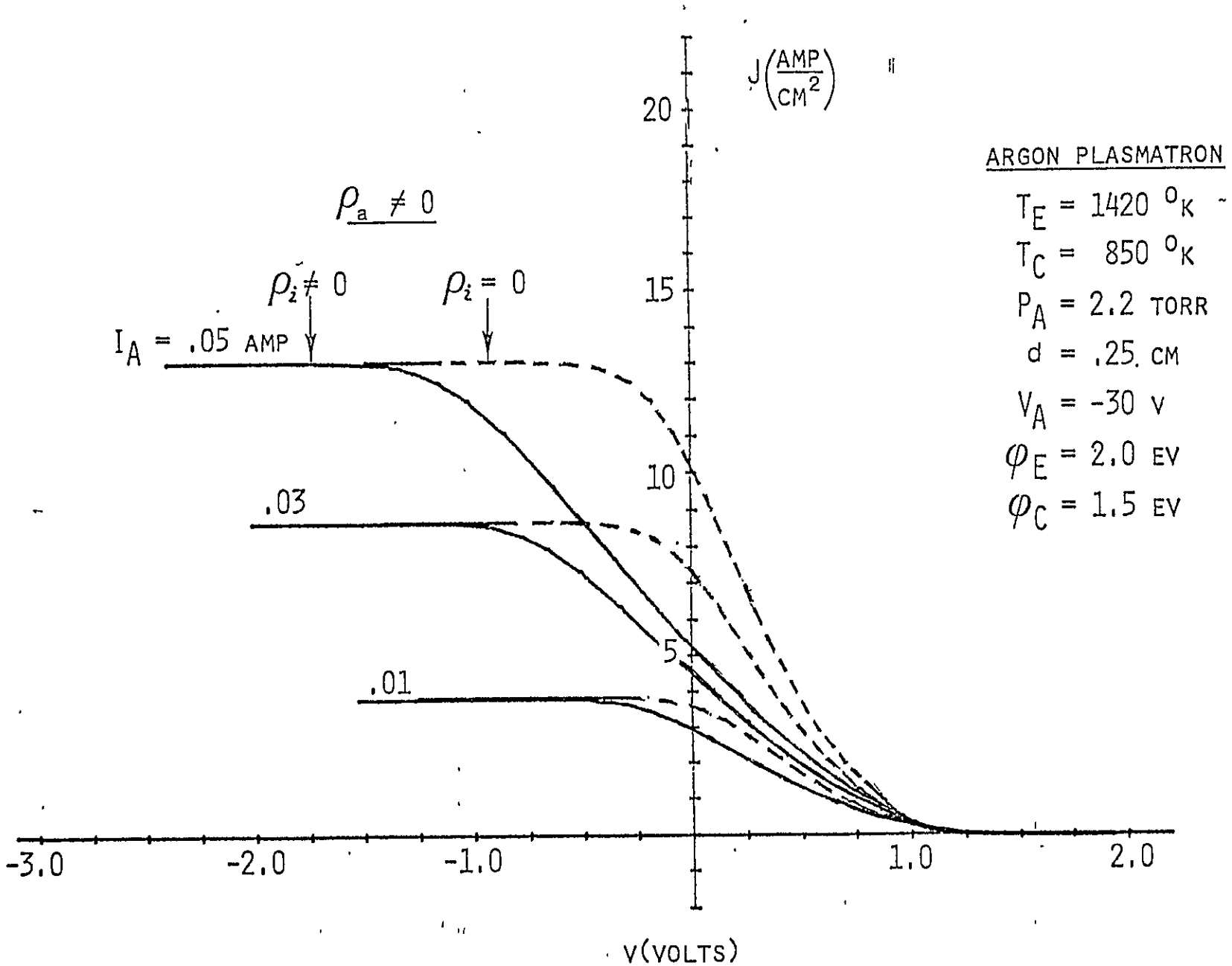

Fig. 13 Calculated Plasmatron J-V Characteristics With and Without Electron-Ion Collisions, (Electron-Atom Collisions Included, $\rho_a \neq 0$).

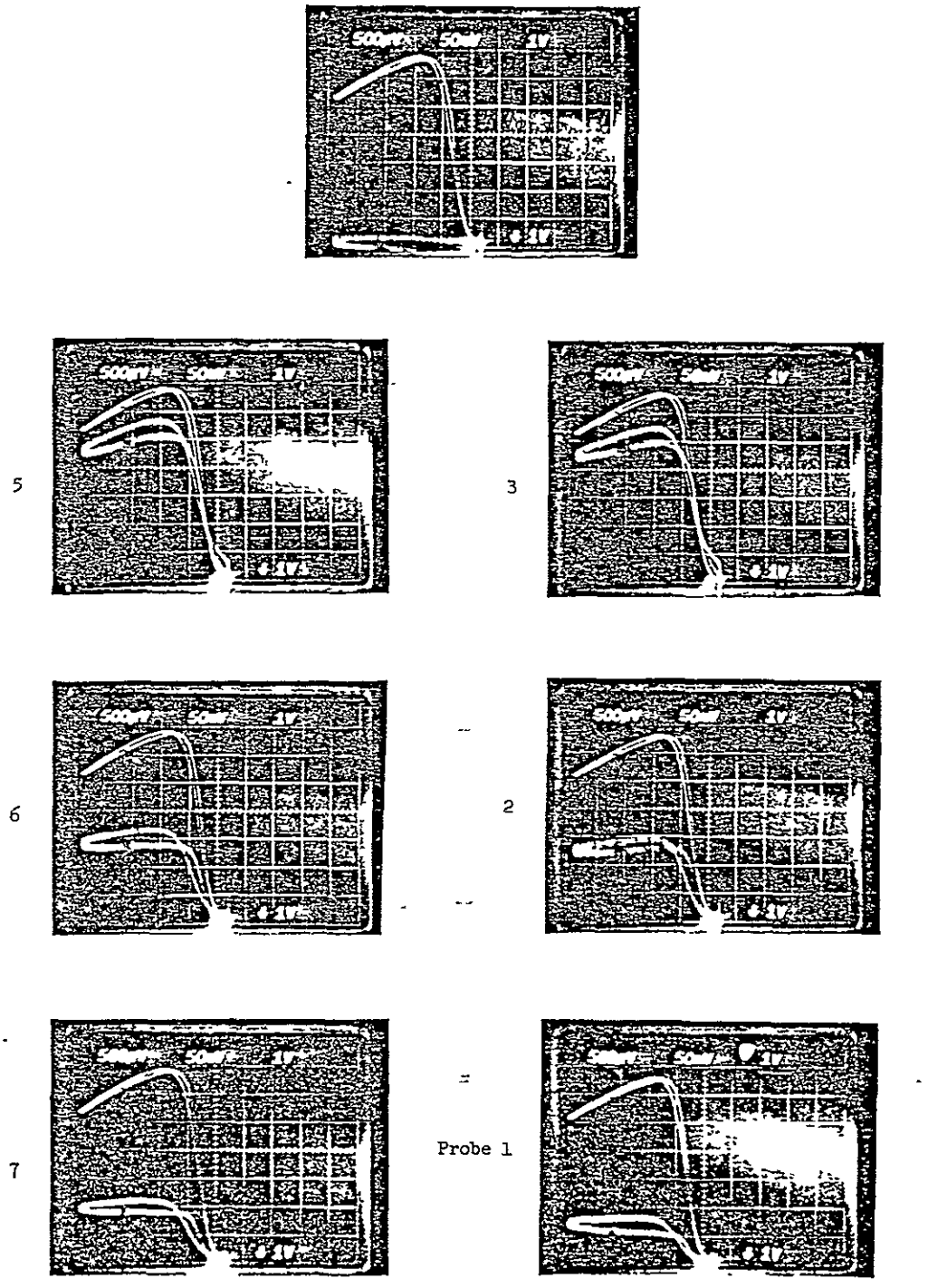

Fig. 14 Converter and Probe Characteristic for the Cylindrical Plasmatron

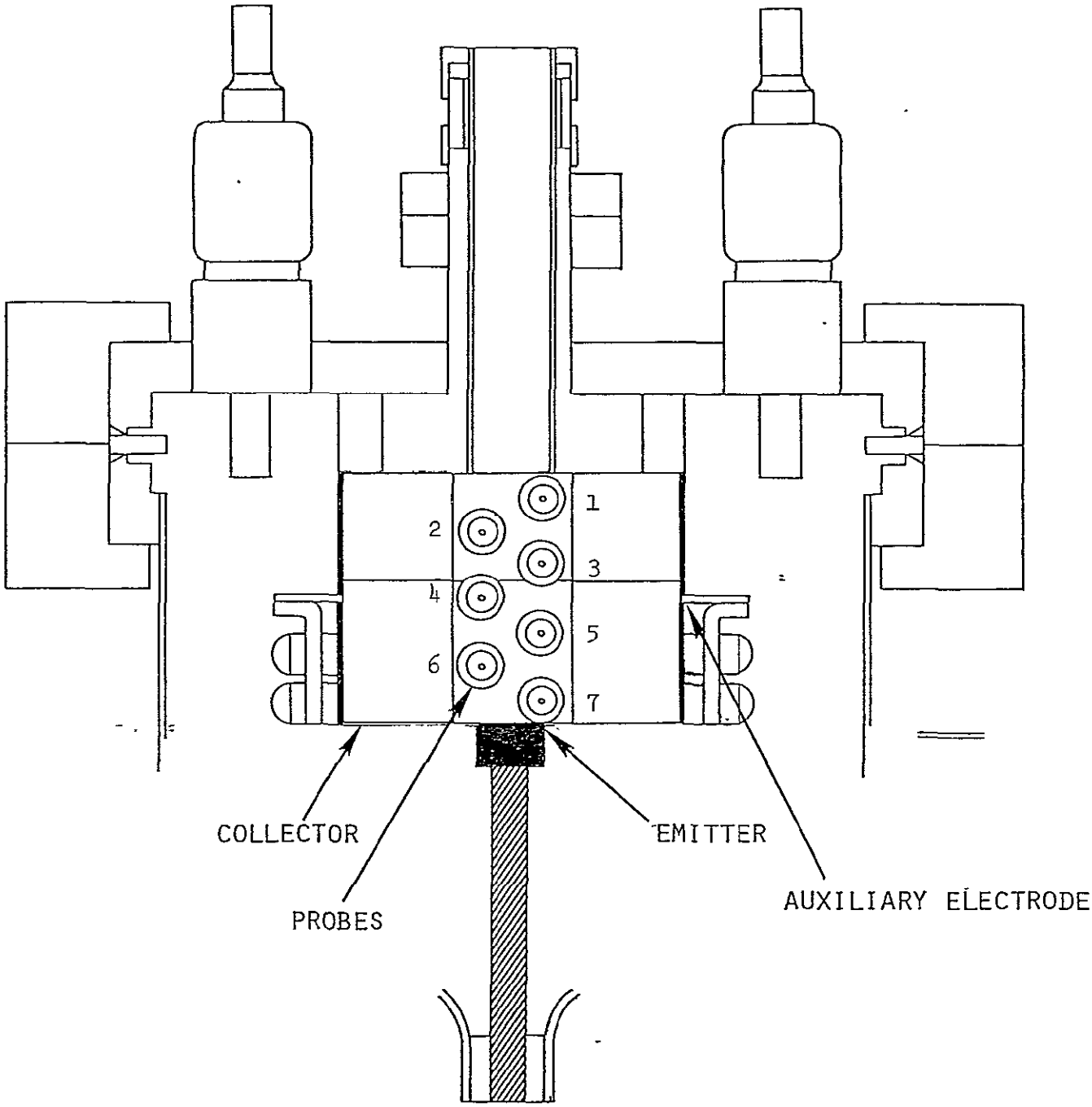

Fig. 15 Probe Positions in the Cylindrical Plasmatron

the interelectrode gap, ion recombination, and the effect of these ions on the converter current density. An example of the net effect is shown in Fig. 16. The positions for the probe current measurements are shown in this figure by the scaled sectional view of the interelectrode space. In this case, no current was observed at the central probe (directly under the auxiliary electrode), but current density in that region was estimated from the total integrated current of the device. Except for the inferred rapid drop-off close to the auxiliary electrode, the current density falls about a factor of 2 for every 2 electrode spacings away from the auxiliary electrode. The ion mean free path in this case is also the same order of magnitude as the interelectrode spacing. It is not known yet whether it is the spacing or the mean free path which most affects the current drop-off. The relative narrowness of the enhancement region indicates that auxiliary electrodes must be closely spaced in a practical device. A similar distribution was obtained earlier by Mayer, et.al.[5], but their results were suspect because of their very narrow emitter. It was not clear whether they were detecting an enhanced current distribution or merely a separation of emitter and auxiliary electrode.

Magnetic Effects

Because the plasmatron is inherently a low pressure device, it is more sensitive to magnetic cut-off than the usual arc-mode converter. This magnetic cut-off for the plasmatron was measured with the cylindrical converter. As mentioned in Chapter III, because of the double ended emitter, current can be passed lengthwise along the emitter to generate an azimuthal magnetic field in the interelectrode space. The observed effect is shown in Fig. 17 where total converter current is plotted versus magnetic flux density. Reduction to 20% of full current occurs at 70 gauss, which corresponds to about 200 amps of axial current. The circular path of an electron with average thermal velocity in a magnetic field would have a diameter equal to the spacing at only 10-20 gauss. That the cut-off is more sluggish than this is probably due to a small amount of interelectrode scattering. Even so, for large advanced mode devices with large currents, this magnetic cut-off could be a serious problem. The problem can probably be removed, however, by appropriate geometric design.

Another magnetic effect, less important for design optimization, is the distortion of the enhanced current distribution due to J x B pumping of the plasma. This is shown by the normalized distributions in Fig. 18. It is interesting to note that the distortion also allows current into the central probe. It would be

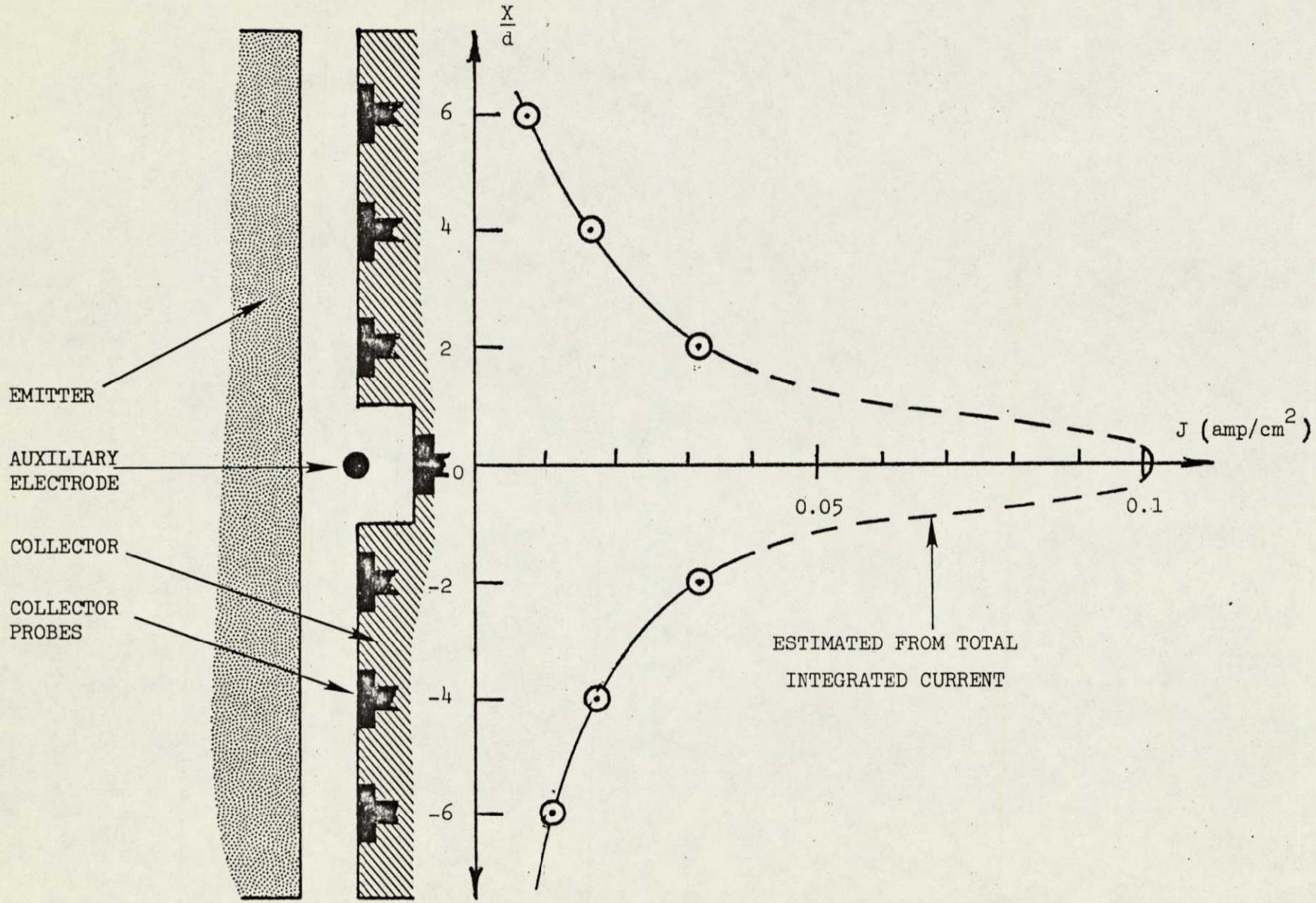

Fig. 16 Enhancement Distribution in the Cylindrical Plasmatron

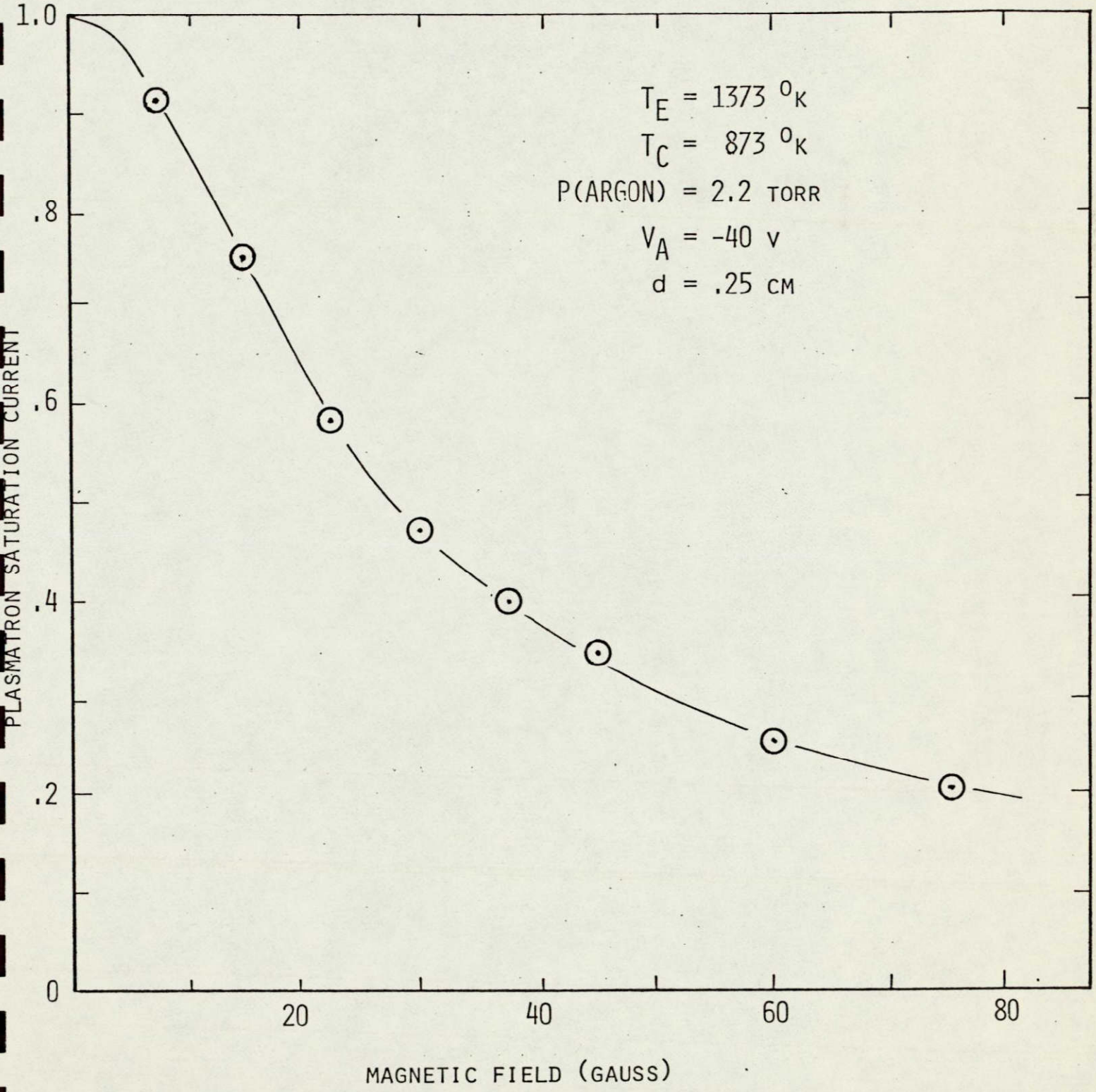

Fig. 17 Magnetic Cut-Off in the Cylindrical Plasmatron

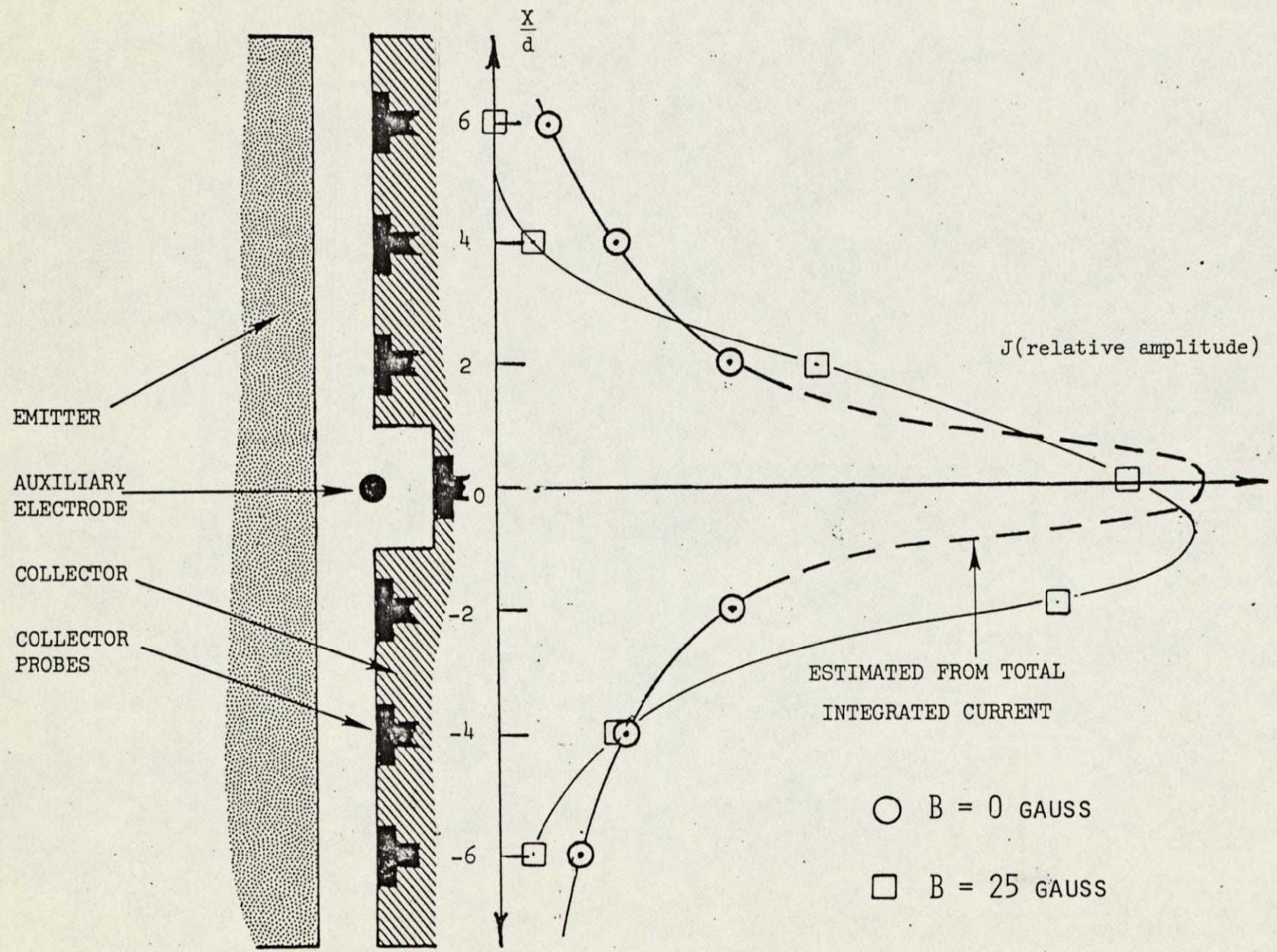

Fig. 18 Magnetic Displacement of the Enhancement Distribution in the Cylindrical Plasmatron

desirable for the J x B pumping to spread the current enhancement down the length of the emitter, since this would reduce the number of auxiliary electrodes needed. Unfortunately, as Fig. 18 shows, the pumping effect is too small to accomplish that.

VI. SOME PRACTICAL IMPLICATIONS

Various thermionic converters and converter modes can be compared using a general performance index Σ defined as

$$\Sigma = kT_E \ln(AT_E^2/J) - V \tag{77}$$

where J and V are the converter current density and output voltage. Σ is directly related to the total of the electron energy losses in the converter, i.e.

$$\Sigma = \phi_C + S + V_d + V_d^* \tag{78}$$

where ϕ_C is the collector work function, and S an equivalent voltage loss due to current attenuation (electron backscatter, surface reflection, non-uniformity, etc.)

$$S = kT_E \ln(J_S/J), \tag{79}$$

V_d the converter arc voltage drop, and V_d^* the equivalent arc drop for external ion production. These voltage losses to the ignited mode converter output, for example, are shown on the motive diagram of Fig. 19. Since S is only an equivalent drop due to current reduction, it appears in Fig. 19 only in terms of the current vectors. But the quantity S appears directly in the current voltage characteristic. This is shown in Fig. 20 where the actual ignited mode characteristic is compared to the idealized characteristic formed by $J = J_S$, (for $V < \phi_E$) and $J = AT_E^2 \exp(-V/kT_E)$, (for $V > \phi_E$). The actual output voltage of the device is reduced from this ideal due to the collector work function ϕ_C and the maintenance voltage (arc drop) for the plasma V_d. The significant reduction of any of these voltage losses leads to advanced performance converters. Part of the output V must be used to supply the equivalent arc drop V_d^* with auxiliary ion source devices, however.

The performance of the elementary (arc-mode) cesium diode converter is characterized by $\Sigma \approx 2.0$ ev. Therefore, the extent to which the performance of any advanced-mode converter is an improvement over the elementary diode is judged by the extent to which the Σ it exhibits is less than 2.0 ev and approaches $\Sigma = \phi_C$ (i.e. the value for which all plasma-related losses are zero).

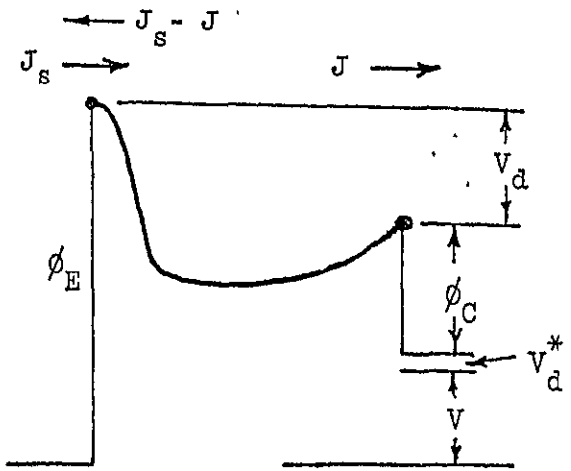

Fig. 19 Potential Parameters for a Converter

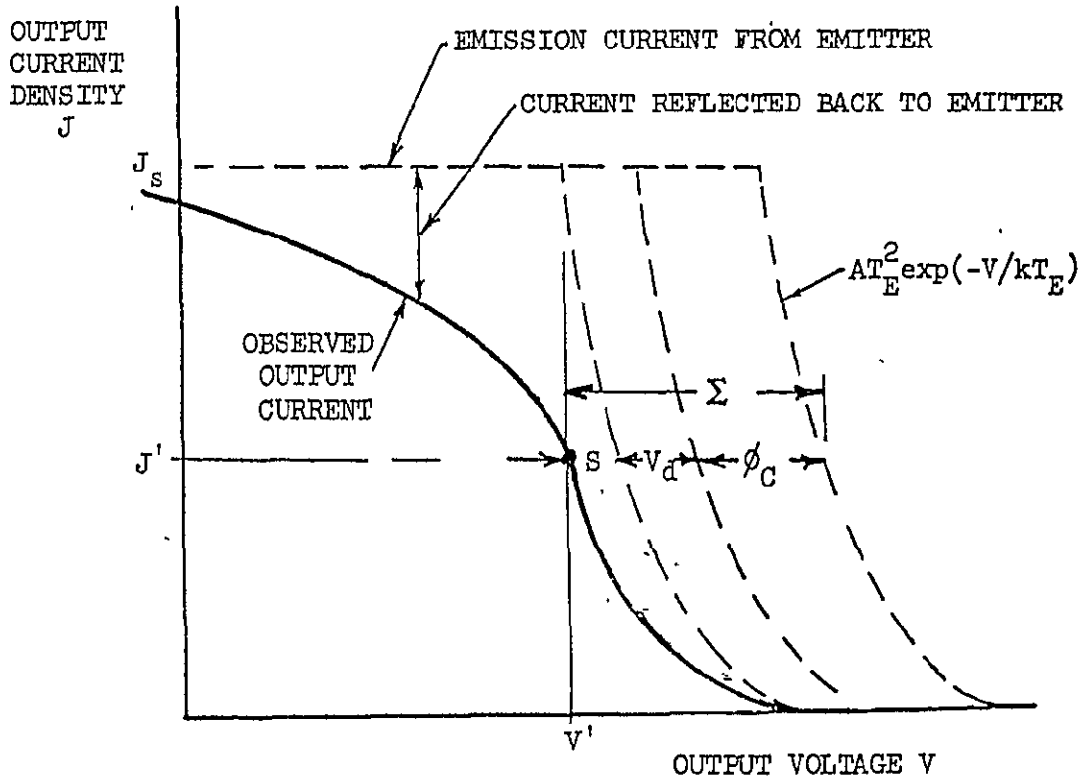

Fig. 20 Voltage Loss Contributions in the Ignited Mode Diode Converter

The curves corresponding to $\Sigma = 2.0$ and $\Sigma = \phi_c = 1.5$ ev are plotted in Figs. 21 and 22, superposed on some performance characteristics for the argon plasmatron. It can be seen that the output of the present argon plasmatron converter (solid curves) is superior to that of the elementary cesium diode converter (i.e. $\Sigma < 2.0$ ev) only at relatively small current densities at the given spacing and temperatures. The corresponding power densities (≤ 1 watt/cm^2, in this case) are too small to be attractive for most practical applications. It is worthwhile, therefore, using the insight provided by the analytical description, to estimate the extent to which undesirable effects encountered in the plasmatron can be suppressed and by what means.

Scattering Reduction

The most beneficial reduction of scattering in the plasmatron would be the reduction of electron-ion scattering. The performance obtained by eliminating this scattering is shown by the dashed curves in Figs. 21 and 22. This could be accomplished by elevating the electron temperature. The gains due to lower plasma resistance will have to be compared with losses due to hot electrons leaving the plasma if the electron temperatures near the electrodes are higher than that of the electrodes. The implications of this approach are presently being studied.

Improvement through reduction of electron-atom scattering is less promising. If the effective ratio of cross sections, of ion production relative to scattering, could be substantially increased beyond even the very favorable ratio for the inert gases, the pressure could be reduced to the point that electron-atom scattering would be negligible. The equivalent of Fig. 21, with electron-atom scattering removed, is given in Fig. 22. As can be seen by comparing the solid curves in Fig. 21 and 22, even complete elimination of electron-atom scattering does not substantially increase plasmatron performance in the practical region $\Sigma < 2$; i.e. electron-atom scattering with argon already is quite small compared with the electron-ion scattering.

In Fig. 22 the dashed curves correspond to the complete absence of scattering effects per se. The remaining voltage difference between these curves and $\Sigma = \phi_c$ occurs because of randomization of electron velocities in the plasma which increases the probability of their returning to the emitter. It is possible that this probability can be modified by structuring the emitter surface[10]. This appraoch to improved performance is also being studied.

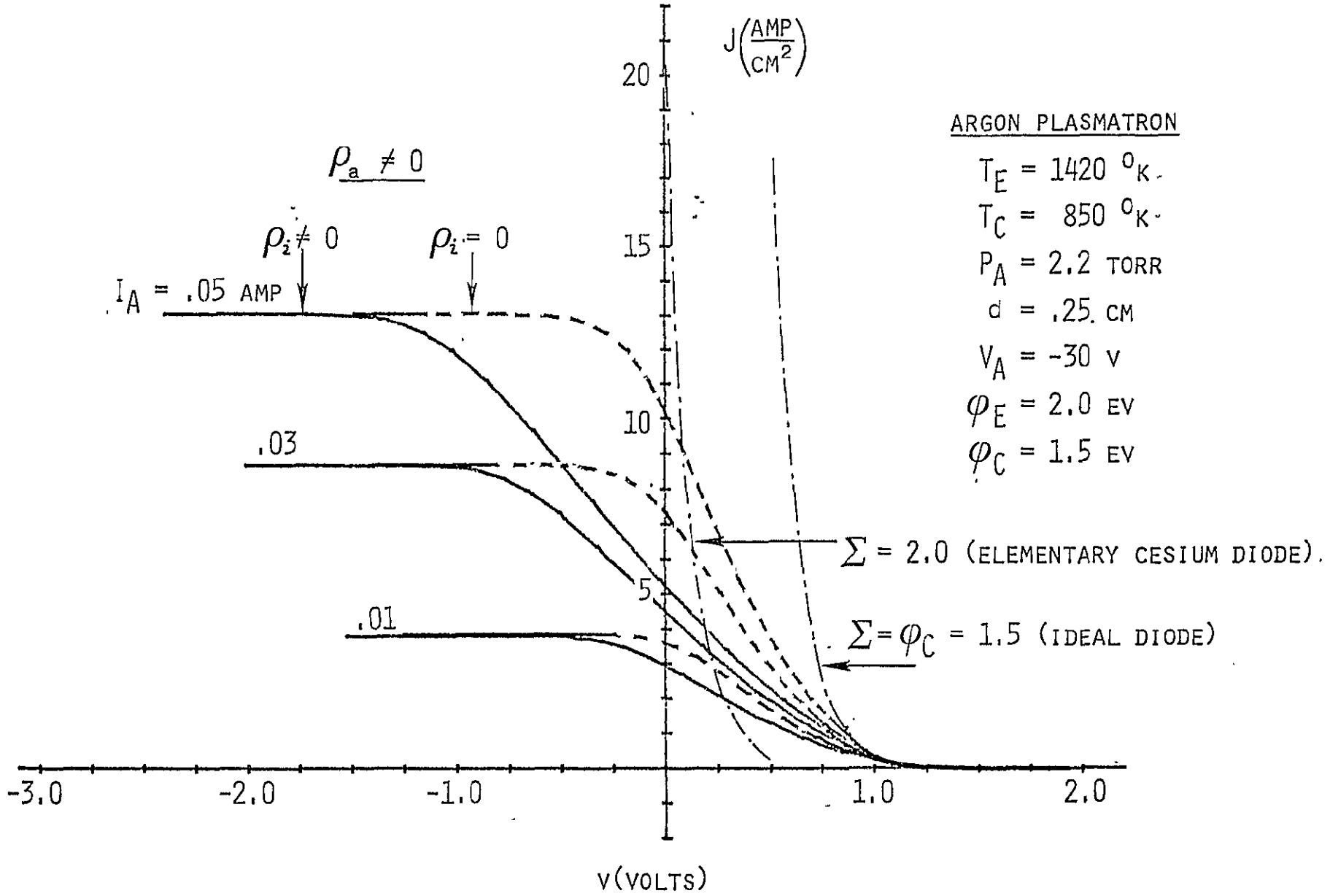

Fig. 21 Calculated Plasmatron J-V Characteristics With and Without Electron-Ion Collisions (Electron-Atom Collisions Included, $\rho_a \neq 0$).

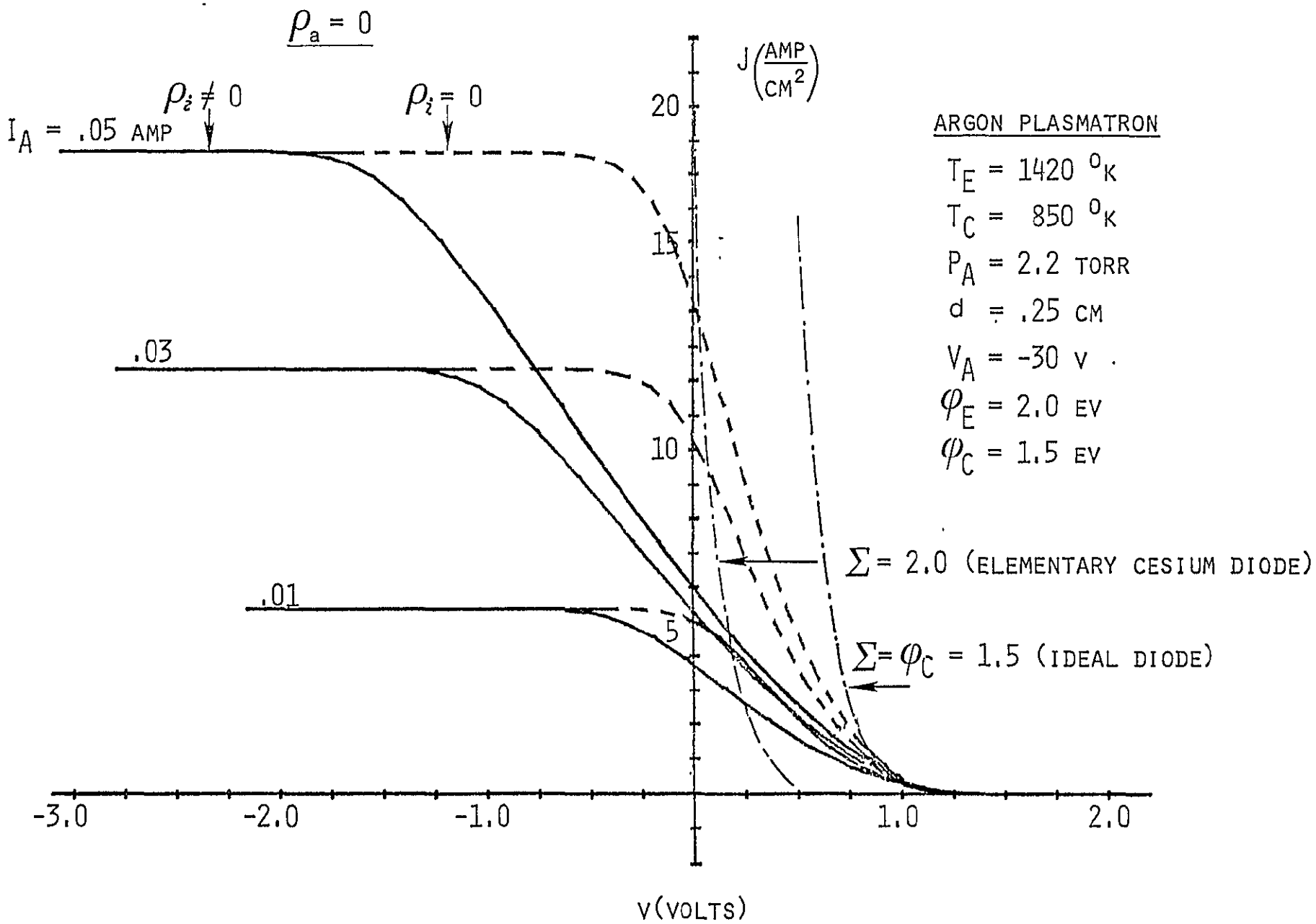

Fig. 22 Calculated Plasmatron J-V Characteristics With and Without Electron-Ion Collisions (Electron-Atom Collisions Excluded, $\Gamma_a = 0$)

Spacing Reduction

The ohmic potential drop arising from electron-ion scattering (i.e. the voltage difference between the solid and dashed curves in Fig. 21 and 22) is proportional to the electrode spacing d. It can be seen, therefore that at electrode spacings less than 0.5 mm, output power densities would be obtained which approach the threshold of practical interest (> 2 watt/cm^2). Elementary cesium diode converters operating with such spacings for many thousand of hours at even higher temperatures already have been reduced to engineering practice. Since the distance between auxiliary emitters cannot greatly exceed the electrode spacing, however, the higher degree of complexity of the plasmatron may make its practical development much more difficult than the diode at small spacings.

Optimum Electrodes

The fact that cesium causes intolerable electron scattering in the plasmatron is unfortunate. These effects can be avoided by using argon for efficient space charge neutralization, but cesium is also very convenient for providing the appropriate emitter and collector work functions. The emitter work function for an advanced performance converter should be low enough ($\approx$ 2 ev) to give ample electron emission ($\geq$ 5 amp/cm^2) at the desired emitter temperatures (1400 - 1600°K). Also, the collector work function should be as low as possible ($\leq$ 1.6 ev).

In past thermionic converters, this appropriate combination of work functions was obtained by cesium adsorption on elementary metal electrodes (tungsten, molybdenum, nickel, etc.). Cesium can still provide these appropriate work functions in an argon plasmatron if the cesium partial pressure can be high enough to give the necessary cesium adsorption, but low enough not to introduce significant undesirable scattering. Whether there is such a compromise partial pressure has not yet been clearly determined. It is known that the cesium pressure required to give an acceptable emitter work function can be greatly decreased by use of an electrode surface which has a high bare work function (e.g., platinum or other platinide metals), or by the use of electronegative gas additives (e.g., oxygen or other chalcogens). Whether this decreased pressure is low enough to avoid the undesirable scattering effects of cesium in an argon plasmatron is being investigated.

If a small partial pressure of cesium cannot be used to obtain appropriate work functions there are other candidate materials which have work functions in

the range of interest. The hexaborides, for example, (particularly of lanthanum) are presently being studied for this purpose. Dispenser emitters like the one used in this study are already available. Unfortunately, the material they dispense poisons the collector and raises its work function to an intolerable 1.8 - 2.1 ev. It is possible, however, that a collector clean-up effect can be introduced (dispensing collector, chemical cycles, collector sputtering, etc.). These possibilities also should be investigated.

VII. CONCLUSIONS

The plasmatron has been evaluated in detail as an advanced performance thermionic converter. Extensive data have been obtained with two experimental devices and detailed calculations have been made using a theory of plasmatron operation developed for this report.

These measurements and calculations show that:

1. The arc drop of the conventional diode thermionic converter can be suppressed by operating the converter as a noble gas plasmatron.

2. This reduction in voltage loss, however, is only effective at low current densities (< 2 amp/cm^2 at practical spacings) because of plasma resistance arising primarily from electron-ion collisions.

3. This plasma resistance loss can be suppressed if the plasma electron temperature is increased or the spacing is reduced. These possibilities are receiving further study.

4. The performance of the argon plasmatron is greatly superior to the cesium plasmatron because electron scattering is intolerably large in cesium at pressures required for efficient ion production in the plasmatron.

5. At present there is no compatible emitter-collector pair of electrodes for use in an argon plasmatron, except for the possibility of using a sufficiently low (negligible scattering) pressure of cesium for adsorption on the electrodes. Electrodes which can operate at such low cesium pressure, or a compatible pair of electrodes which can operate without cesium vapor, should be sought.

6. Magnetic cutoff must be considered in the design of plasmatron converters with high output currents.

7. A sufficiently dense plasma for practical output current is maintained only about one to two gap widths from the auxiliary emitter in the plasmatron. This implies that in practical converters the spacing between auxiliary emitters cannot be much greater than a few gap widths The practical implications of the observed zero-current "shadow" of the auxiliary electrode on the collector should be investigated.

Better understanding of the plasmatron thermionic converter -- and improved performance -- are objectives of the continuing project. This will be approached by obtaining further experimental data required to improve the theory and to evaluate the plasmatron innovations suggested by the theory. The theory will be used also to define the optimum operating conditions for maximum plasmatron performance.

SYMBOLS

A = current amplification factor [Eq.(74), p. 31]

$A,B,C,$ = coefficients in equation for plasmatron current [Eq.(45), p. 21]

D_a = ambipolar diffusion coefficient [Eq. (7), p. 14]

D_e = electron diffusion coefficient

D_p = ion diffusion coefficient

d = interelectrode spacing

e = fundamental charge

$I(A)$ = auxiliary electrode current

I_A = auxiliary electrode current

I_S = saturation current

J = current density of a converter

$J_R(E)$ = Richardson electron emission flux from the emitter

J_S = saturation current density from an emitter

k = Boltzmann constant

M = ion mass

m = electron mass

N_a = atom density

n = plasma density

n_E = plasma density near the emitter

P = gas pressure

P_C = elastic collision probability

Q = flux ratio [Eq. (36), p. 19]

R = flux ratio [Eq. (35), p. 19]

S = equivalent voltage loss due to current attenuation [Eq.(79), p. 47]

S = ionization coefficient [Eq. (5), p. 14]

T_C = collector temperature

T_E = emitter temperature

T_e = electron temperature in the plasma

T_{eE} = electron temperature in the plasma near the emitter

T_p = ion temperature in the plasma

T_{pE} = ion temperature in the plasma near the emitter

T_R = cesium reservoir

V = output voltage

V = plasma potential

V_A = applied voltage bias to auxiliary electrode

V_B = auxiliary electrode bias

V_C = collector sheath potential drop

V_d = interelectrode voltage drop

V_d^* = equivalent voltage drop [Eq. (75), p. 31]

V_E = emitter sheath potential drop

V_o = plasmatron output voltage

V_p = potential drop across the plasma

V_i = ionization potential

v_e = mean velocity of electrons

v_{eE} = mean electron velocity in the plasma near the emitter

v_p = mean velocity of ions

v_{pE} = mean ion velocity in the plasma near the emitter

w = normalized collector flux [Eq. (46), p. 21]

x = distance from the emitter

$\alpha_o, \alpha_1, \alpha_2$ = coefficients for density distribution [Eq. (8), p. 14]

β^* = ionization probability for an atom or ion incident to a surface

β_E = emitter ion-richness emission ratio

Γ_+ = electron random flux in the positive direction

Γ_- = electron random flux in the negative direction

Γ_e = electron flux in the plasma

Γ_{eC} = electron flux in the plasma near the collector

Γ_{eE} = electron flux in the plasma near the emitter

Γ_p = ion flux in the plasma

Γ_{pE} = ion flux in the plasma near the emitter

Γ_{pC} = ion flux in the plasma near the collector

Δ = parameter in plasmatron solution [Eq. (42), p. 20]

Δ' = parameter in plasmatron solution [Eq. (51), p. 22]

Λ = parameter in plasma resistivity expression (see pp. 12 and 13)

λ_a = equivalent ion mean free path corresponding to ambipolar diffusion coefficient D_a [Eq. (44), p. 21]

λ_e = electron mean free path

λ_p = ion mean free path

μ_a = atom arrival rate for cesium [Eq. (56), p. 23]

μ_e = electron mobility

μ_o = ion mobility coefficient

μ_p = ion mobility

ν_e = Richardson electron emission flux from the emitter

ν_p = ion emission flux from the emitter

ξ = parameter in plasmatron solution [Eq. (43), p. 21]

ρ_a = plasma resistivity due to electron-atom collisions

ρ_i = plasma resistivity due to electron-ion collisions

Σ = performance index [Eqs. (77) and (78), p. 47]

σ_i = ionization cross section

ϕ_A = auxiliary electrode work function

ϕ_C = collector work function

ϕ_E = emitter work function

REFERENCES

1. N.S. Rasor, L.K. Hansen, G.O. Fitzpatrick, and E.J. Britt, 10th Intersociety Energy Conversion Engineering Conference, Newark (1975), 367.

2. L.K. Hansen and N.S. Rasor, 1975 Thermionic Conversion Specialists Meeting, Eindhoven.

3. W. Bloss, Advanced Energy Conversion 3 (1963) 315.

4. R.C. Knechtli and M. Fox; ibid, 333.

5. R. Mayer, H. Jungclaus, and R. Pruschek, 1st Intl. Conf. on Thermionic Elect. Pwr. Generation, London, England (1965).

6. H. Albrecht, B. Saggau, and H. Strecker, 2nd Intl. Conf. on Thermionic Elect. Pwr. Generation, Stresa, Italy (1968) 1108.

7. G. Ecker, "Gas Discharge Theory", in Advanced Plasma Theory, M.N. Rosenbluth, Ed., Academic Press, New York, (1964) p 97.

8. L. Spitzer, "Physics of Fully Ionized Gases", Interscience Publishers, New York, 1956, p. 84.

9. I.P. Shkarofsky, T.W. Johnston, and M.P. Bachynski, "The Particle Kinetics of Plasmas", Addison-Wesley, Reading, Mass., 1966, p. 263.

10. C. Warner and L.K. Hansen, "Transport Effect in the Electron-Rich Unignited Mode of Cesium Diodes", J. Appl. Phys. 38, 491 (1967).

11. J.M. Houston, Report on Thermionic Conversion Specialist Conference, IEEE, Cleveland, 1964, p. 300.

12. M. Gryzinski, Phys. Rev. 138, A336 (1965).

PAPERS PRESENTED

1. L.K. Hansen and N.S. Rasor, "Advanced Mode Thermionic Converters", Proceedings, 1975 Thermionic Conversion Specialists Meeting, Eindhoven University of Technology, Eindhoven, Sept. 1975, p. 209.

2. L.K. Hansen and N.S. Rasor, "Advanced Thermionic Converter Operating Modes", (abstract only) Conference Record-Abstracts, The 1976 IEEE International Conference on Plasma Science, University of Texas at Austin, Austin, Texas, May 1976, p. 139.

3. L.K. Hansen and N.S. Rasor, (oral presentation only) Thermionic Conversion Contractors Review Meeting, Austin, Texas, May 1976.

4. L.K. Hansen, G.L. Hatch, G.O. Fitzpatrick, and N.S. Rasor, "The Plasmatron as an Advanced Performance Thermionic Converter", Eleventh Intersociety Energy Conversion Engineering Conference Proceedings, Stateline, Nevada, Sept. 1976, Vol. II, p 1630.